International Journal of Climatology

International Journal of Climatology RMetS

RESEARCH ARTICLE OPEN ACCESS

ENSO Diversity Regulation of the Impact of MJO on Extreme Snowfall Events in the Peruvian Andes

Juan Sulca[1,2]

[1]Instituto Geofísico del Perú, Lima, Peru | [2]Universidad Nacional de Ingeniería, Lima, Peru

Correspondence: Juan Sulca (sulcaf5@gmail.com)

Received: 21 November 2023 | **Revised:** 2 February 2025 | **Accepted:** 5 February 2025

Funding: This work was supported by Consejo Nacional de Ciencia, Tecnologia e Innovación Tecnologica del Perú (CONCYTEC) through the PROCIENCIA program as part of the "Becas en programas de doctorado en alianzas interinstitucionales" (contract PE501093367-2024-PROCIENCIA-BM) and the "Concurso Alianzas Interinstitucionales para Programas de Doctorado" (contract PE501084296-2023-PROCIENCIA-BM) and Peruvian PPR 068 program" Reduccion de vulnerabilidad y atención de emergencias por desastres.

Keywords: Bolivian high-Nordeste low system | ENSO diversity | extratropical Rossby wave train | extreme snowfall events | MJO | moisture transport | Peruvian Andes

ABSTRACT

Extreme snowfall events (ESEs) in the Peruvian Andes (10°–18.4° S, >4000 m) result in considerable economic losses. Despite their importance, how El Niño-Southern Oscillation (ENSO) diversity modulates the impact of the Madden–Julian Oscillation (MJO) on ESEs in the Peruvian Andes remains unexplored. Daily ERA5 reanalysis data from 1981 to 2018 were analysed. This study examines 16 ESEs. A bandpass filter with a 20–90-day range was applied to isolate the intraseasonal component of the daily anomalies. Additionally, time series data from the real-time multivariate MJO (RMM) index and Eastern and Central ENSO (E and C) indices were utilised. Composites were performed to describe the atmospheric circulation patterns related to ESEs in the Peruvian Andes under neutral, El Niño and La Niña conditions in the central and eastern Pacific Ocean. Under non-ENSO conditions, the MJO alone does not trigger ESEs in the Peruvian Andes during the DJF season. The absence of a well-organised convection system over the Peruvian Andes prevents ESEs. Conversely, during the JJA season, MJO Phases 5, 6 and 7 induce ESEs in the southern Peruvian Andes by enhancing moisture flux from the east through the equatorward propagation of an extratropical Rossby wave train that crosses South America and reaches the Altiplano region. In terms of ENSO diversity, the combined effects of the Central La Niña and MJO Phases 6 + 7 induce ESEs across the Western Cordillera of the southern Peruvian Andes during the DJF season. During austral winter, the interaction between the Central El Niño and MJO Phases 8 + 1, Eastern El Niño and MJO Phases 2 + 3, and Eastern La Niña and MJO Phases 8 + 1 induce ESEs across the Peruvian Andes.

1 | Introduction

In austral summer (DJF), the greatest amount of precipitation occurs over the south-central Amazon. The South Atlantic convergence zone (SACZ), oriented northwest-southeast, generates a cloud band with intensified precipitation, which seems to integrate with the vigorous convection over the Amazon Basin, extending from tropical South America (SA) southeastward into the South Atlantic Ocean (Kodama 1992; Liebmann et al. 1999; Grimm 2019). The primary characteristic of low-level circulation over South America is the South American low-level jet (SALLJ), which is situated east of the Andes and facilitates the transport of warm and moist air from the Amazon Basin toward the subtropics (Montini et al. 2019). In the upper troposphere, at approximately 200 hPa, the predominant feature of the atmospheric circulation over the South American continent is the Bolivian high-Nordeste low (BH-NL) system (Chen et al. 1999). The liberation of latent heat during convection over

the Amazon Basin establishes the core structure of the BH-NL system (Lenters and Cook 1997). Additionally, Chen et al. (1999) reported that warm sea surface temperature (SST) anomalies in the southeastern tropical Atlantic intensify the upper-level BH-NL system. The BH-NL system is absent during austral winter, when the upper-level westerly zonal flow prevails over South America.

Glaciers in the Andes Mountains serve as essential buffers against seasonal precipitation variability, supplying water for domestic, agricultural, and industrial uses during dry periods (Vuille et al. 2008). However, there is limited research on the climatological characteristics of snowfall events in the Andes Mountains. In the northern Chilean Andes, Vuille and Ammann (1997) observed that cutoff lows and the northward movement of cold Pacific air masses cause snowfall during the winter months (May–September) over a six-year period (1984, 1986, and 1990–1993). Conversely, few studies have investigated snowfall in the Peruvian Andes (above 3800 m), which is influenced by changes in South America's regional atmospheric circulation. During the wet months (October–March), the Peruvian Andes experience snowfall, but the underlying physical mechanisms differ (Aliaga-Nestares et al. 2021; Hurley et al. 2015). For example, Aliaga-Nestares et al. (2021) utilised the elbow method in cluster K-means analysis to identify two distinct atmospheric circulation patterns for wet ESEs in the Peruvian Andes associated with changes in the Bolivian high's intensity and position. Type-1 wet ESEs in the Peruvian Andes are characterised by a strengthened Bolivian high, resulting in upper-level northeasterly wind anomalies that increase moisture transport from the Amazon to the Andes. In Type-2 wet ESEs, an upper-level trough near the Peruvian coast (85° W, 10° S) shifts the Bolivian high eastward from its typical position (60° W, 15° S). This configuration leads to southwesterly wind anomalies over the Andes in Peru and Bolivia, indicating enhanced moisture flow from the Amazon Basin to the central Andes (Garreaud et al. 2003; Vuille and Keimig 2004; Imfeld et al. 2019; Segura et al. 2019; Villalobos-Puma et al. 2022). Although these two types of upper-level atmospheric circulation patterns for wet ESEs in the Peruvian Andes have been identified, the underlying large-scale phenomena remain unclear. Conversely, Hurley et al. (2015) reported that cold surges propagating along the eastern slope of the Andes account for approximately 70% of the total snow accumulation on the Quelccaya Ice Cap in the Peruvian Andes at an elevation of 5680 m. However, no study has identified the predominance of any of these three mechanisms in causing extreme snowfall events in the Peruvian Andes during the DJF season.

Numerous case studies indicate that in the southern Peruvian Andes, snowfall during the dry months (April–September) results from mainly synoptic processes (Quispe and Avalos 2006a; Quispe and Avalos 2006b; Quispe 2014; Quispe 2017; Aliaga-Nestares et al. 2021). Recently, Aliaga-Nestares et al. (2021) identified three atmospheric circulation patterns that characterise winter ESEs in the Peruvian Andes. Type-1 dry ESEs in the Peruvian Andes feature a convergence of an upper-level trough near the coasts of Peru and northern Chile (82° W, 8° S) at 300 hPa. This condition leads to upper-level southwesterly wind anomalies over the Andes in Peru and Bolivia, increasing moisture transport from the Amazon Basin to the central Andes, thereby initiating instability and causing snowfall. Type-2 dry ESEs are marked by an upper-level cutoff low (77° W, 22° S), which causes southwesterly wind anomalies over the Andes in Peru and Bolivia. This condition amplifies the moisture flow from the Amazon Basin to the central Andes, leading to instability and the onset of snowfall. In Type-3 dry ESEs, an upper-level trough near the coast of Peru and northern Chile (75° W, 15° S) transports a cold and dry Pacific air mass to the central Andes. This leads to enough instability to trigger snowfall in the region.

El Niño-Southern Oscillation (ENSO) is the primary driver of interannual variability in global temperature and precipitation. ENSO has warm and cold phases of sea surface temperature (SST), known as El Niño and La Niña, respectively. Several studies have shown that ENSO modulates the height, size and intensity of precipitation events (Liu et al. 2019). Using the multivariate ENSO index, Liu et al. (2019) noted that El Niño inhibits the initiation of mesoscale convection systems and simultaneously reduces the height of the column of deep convection over the Amazon Basin and in the tropical Andes, tropical Atlantic and even the subtropics. In Peru, for example, Lagos et al. (2008) reported that warm Niño 3.4 episodes cause rainfall along the northern Peruvian coast, whereas they reduce rainfall along the Peruvian Andes. Conversely, La Niña tends to exhibit the opposite pattern related to El Niño.

Since ENSO induces extreme rainfall events worldwide, the scientific community has identified specific regions in the equatorial Pacific Ocean that capture ENSO signals. These regions are Niño 1 + 2 (N1 + 2; 0°–10° S, 90°–80° W), Niño 3 (N3; 5° S–5° N, 150°–90° W), Niño 3.4 (N3.4; 5° S–5° N, 170°–120° W), and Niño 4 (N4; 5° S–5° N, 160°–150° W). These regions are used to develop statistical forecast models and monitor ENSO. For example, Lagos et al. (2008) developed a forecast model for December rainfall on the northern coast of Peru using December SST predictions from the Niño 3.4 region. Similarly, Wu et al. (2018) used the Niño 3.4 index as a predictor for forecasting rainfall in the southern Peruvian Andes. Conversely, La Niña tends to exhibit the opposite pattern related to El Niño. In addition, the authors reported that changes in SST anomalies in the tropical Atlantic Ocean do not modulate summer rainfall in the southern Peruvian Andes. In subtropical regions, La Niña weakens the intensity of the intertropical convergence zone, thereby reducing upper-level convergence in the subtropics. Thus, La Niña conditions promote the intrusion of extratropical Rossby wave trains into the South American continent (Barreiro 2016).

In recent decades, numerous studies have highlighted the necessity of employing two independent indices to characterise the nonlinear behaviour of ENSO (Takahashi et al. 2011; Capotondi et al. 2015; Tedeschi et al. 2015, 2016; Goudard et al. 2024). Takahashi et al. (2011), using rotated empirical orthogonal function techniques, reported that Eastern and Central El Niño events are associated with warm SST anomalies confined to the eastern and central Pacific Ocean. However, these phenomena exert different impacts on large-scale atmospheric circulation over South America. In tropical regions, Sulca et al. (2018) emphasised that both Eastern and Central

El Niño events generate an upper-level stationary Rossby wave over the Pacific Ocean at 200 hPa. Upper-level easterly wind anomalies dominate the equatorial Pacific, whereas upper-level westerly wind anomalies are observed over the tropical Andes, leading to dry conditions in these regions. The magnitude of upper-level westerly wind anomalies over Peru is twice as large during Central El Niño events. Conversely, the two types of La Niña exhibit upper-level regional atmospheric patterns opposite to those associated with the two types of El Niño. Sulca et al. (2021), using a statistical rainfall model, reported that summer rainfall in the Eastern Cordillera of the Peruvian Andes cannot be explained solely by the variability of the equatorial Pacific Ocean. Goudard et al. (2024), using classical SST El Niño regions, reported that warm SST anomalies in the Niño 4 region (Central El Niño) induce an upper-level Rossby wave train over the Pacific Basin, but it is twice as weak as that in the warm SST Niño 3 region. This result contrasts with reported upper-level atmospheric circulation over the Central and Eastern SST Niño indices (Sulca et al. 2018).

The Madden–Julian Oscillation (MJO) is a large-scale anomalous atmospheric circulation that originates in the western Indian Ocean and is confined to the tropics. It has the characteristic of propagating toward the east with a speed that varies between 5 and 10 $m\,s^{-1}$. The MJO has periods of between 30 and 90 days (Madden and Julian 1972, 1994), and its maximum intensity occurs twice a year: in summer and autumn in the Southern Hemisphere. This wave disturbance has an eastward propagation of tropical convective anomalies from the Indian Ocean to the western Pacific and subsequently to South America and Africa.

Numerous studies have investigated the influence of the MJO on extreme rainfall episodes in South America, focusing on its effects on upper-level atmospheric circulation (Madden and Julian 1972; Alvarez et al. 2016; Grimm 2019; Mayta et al. 2019; Recalde-Coronel et al. 2020; Liu et al. 2023; Fernandes and Grimm 2023). For example, Grimm (2019) reported that MJO Phases 8 + 1 increase precipitation in subtropical South America at approximately 30° S by generating upper-level anticyclonic and cyclonic circulation patterns. In the Peruvian Andes, Recalde-Coronel et al. (2020) reported that MJO Phases 8 + 1 reduce rainfall over the Western Cordillera of the southern Peruvian Andes from 1981 to 2016.

Few studies have examined how different ENSO types regulate the MJO teleconnection (Moon et al. 2011; Alvarez et al. 2016; Shimizu and Ambrizzi 2016; Shimizu et al. 2017). Using the Niño 3.4 index, Moon et al. (2011) analysed how neutral, El Niño and La Niña conditions influence MJO Phases 3 and 7 on upper-level atmospheric circulation over South America north of 40° S during the period 1979–2008. Under neutral ENSO conditions, MJO Phase 3 enhances the upper-level BH-NL system over South America by strengthening deep convection over the Indian Ocean and the African continent, which intensifies the upper-level eastern zonal flow. This corresponds to a significant OLR dipole, with positive anomalies over northeastern Brazil and negative anomalies over the southern Peruvian Andes. El Niño negates the remote influence of MJO Phase 3 on the Peruvian Andes by inducing upper-level flow anomalies north of 22° S in South America. Conversely, La Niña strengthens the teleconnection of MJO Phase 3 over South America by amplifying and expanding upper-level easterly flow anomalies latitudinally over South America, which is indicative of an enhanced upper-level BH-NL system. MJO Phase 7 reduces upper-level easterly flow over equatorial South America (10° N–8° S) and enhances the Bolivian High via the eastward propagation of extratropical Rossby wave trains into the South American continent. El Niño intensifies and expands toward the south of the upper-level flow anomalies over South America, indicating a weakening of the BH-NL system. Conversely, La Niña neutralises the effect of MJO Phase 7 on upper-level atmospheric circulation over South America by intensifying the upper-level easterly flow over SA. Under MJO Phase 7, La Niña induces wet anomalies over the Altiplano region via eastward propagation of extratropical Rossby wave trains into the South American continent, provoking a slightly enhanced Bolivian High. In contrast, no studies have assessed the impacts of the MJO on extreme snowfall events in the Peruvian Andes under different types of SST configurations over the equatorial Pacific (e.g., Eastern and Central ENSO).

The main goal of this study is to elucidate whether the coupling of the MJO and ENSO induces extreme snowfall events in the entire Peruvian Andes by examining alterations in large-scale atmospheric circulation patterns over the Southern Hemisphere. This study focuses on the DJF and JJA seasons because the patterns of low- and upper-level atmospheric circulation associated with the MJO are unstable in the transition seasons (Fernandes and Grimm 2023).

2 | Data and Methods

This study extracts the list of extreme snowfall events for the summer (DJF) and winter (JJA) seasons from Aliaga-Nestares et al. (2021) (Table 1). The details of the definition and identification of extreme snowfall events in the Peruvian Andes are documented in Aliaga-Nestares et al. (2021).

Daily gridded precipitation data from the Peruvian Interpolated Data of the Servicio Nacional de Meteorología e Hidrología (SENAMHI) Climatological and Hydrological Observations version 2.1 (PISCOp v2.1; Aybar et al. 2020; Gutierrez et al. 2022) dataset were used to verify the occurrence of wet episodes during extreme snowfall events in the Peruvian Andes. PISCOp v2.1 has a horizontal resolution of 10 × 10 km and covers the 1981–2018 period. This dataset can be downloaded at https://figshare.com/articles/dataset/High-resolution_gridded_rainfall_dataset_for_Peru_-_PISCOp_v2_2_dataset/21127423.

The ERA5 reanalysis (Hersbach et al. 2020) from the European Centre for Medium-Range Weather Forecasts (ECMWF) was used to characterise the snowfall and 200-hPa geopotential height and wind daily patterns associated with the MJO. This analysis has a resolution of 31 km and covers the same 1981–2018 period.

To study the deep convection associated with extreme snowfall events in the Peruvian Andes, daily OLR data from the NCAR/National Oceanic and Atmospheric Administration (NOAA)

TABLE 1 | List of extreme snowfall events in the Peruvian Andes during austral summer (DJF) and winter (JJA) from 1995 to 2018. Only RMM Phases with a module higher than or equal to 1 are shown. Only Eastern and Central El Niño (La Niña) with values greater than or equal to 1 are shown. This list was extracted from Aliaga-Nestares et al. (2021).

DJF				JJA			
Event	**Date**	**MJO phase**	**ENSO type**	**Event**	**Date**	**MJO phase**	**ENSO type**
1	12/27/1995	—	E^{-}	**1**	08/07/1997	—	E+
2	12/03/1999	4	C^{-}	**2**	08/21/1997	—	E+
3	01/23/2004	2	C^{+}	**3**	07/10/2002	7	C+
4	12/31/2007	5	E− C−	**4**	06/28/2004	7	—
5	12/21/2008	—	C−	**5**	07/01/2004	8	—
6	02/17/2009	—	C−	**6**	07/02/2004	8	—
7	01/10/2010	—	C+	**7**	07/03/2004	8	—
8	02/12/2011	—	C−	**8**	07/04/2004	8	—
9	12/21/2011	4	C−	**9**	08/23/2004	8	C+
10	12/23/2011	4	C−	**10**	08/24/2004	8	C+
11	12/24/2011	5	C−	**11**	08/08/2008	2	E+ C−
12	12/25/2011	5	C−	**12**	07/26/2009	—	—
13	01/05/2012	—	C−	**13**	07/27/2009	—	—
14	01/06/2012	—	C−	**14**	07/03/2011	—	C−
15	01/27/2012	6	C−	**15**	06/07/2012	5	E+
16	01/29/2012	6	C−	**16**	08/24/2013	8	E−
17	02/06/2012	7	C−	**17**	08/25/2013	8	E−
18	02/09/2012	8	C−	**18**	08/27/2013	1	E−
19	02/12/2012	8	C−	**19**	08/28/2013	1	E−
20	02/20/2012	2	C−	**20**	08/29/2013	1	E−
21	01/17/2013	7	—	**21**	07/03/2015	7	E+
22	01/22/2013	7	—	**22**	07/04/2015	7	E+
23	01/16/2014	—	—	**23**	08/12/2015	—	E+ C+
24	01/04/2015	7	C+	**24**	08/13/2015	—	E+ C+
25	01/20/2015	7	C+	**25**	06/28/2016	—	—
				26	07/07/2016	—	—
				27	06/03/2018	5	—
				28	06/04/2018	5	—
				29	06/05/2018	5	—
				30	07/14/2018	5	—
				31	07/19/2018	5	—
				32	07/20/2018	6	—
				33	07/21/2018	6	—
				34	07/22/2018	6	—
				35	08/07/2018	6	—

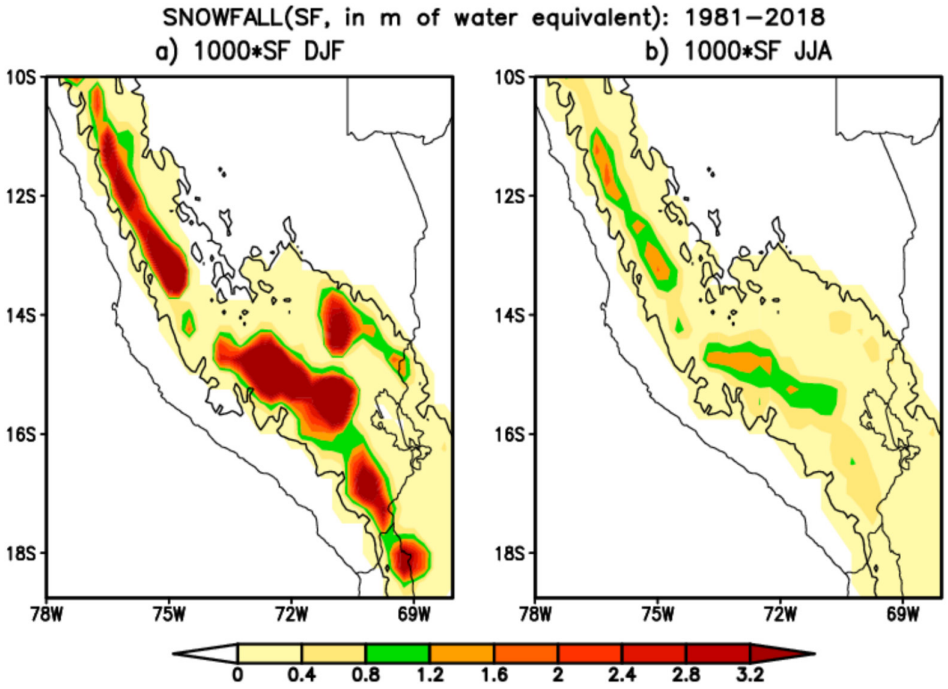

FIGURE 1 | Climatology of snowfall (in m of water equivalent) during (a) austral summer (December–January–February, DJF) and (b) austral winter (June–July–August, JJA). The climatology is based on the period from 1981 to 2010. The ERA5 reanalysis was used in this analysis. [Colour figure can be viewed at wileyonlinelibrary.com]

(Liebmann and Smith 1996) for the period 1981–2018 were analysed.

The daily anomalies were calculated by removing the mean and its first three harmonics, from which the linear trend was also removed. On the other hand, a 20–90-day bandpass filter based on the Morlet wavelet (Torrence and Compo 1998) was applied to extract the intraseasonal component of the data. This band was chosen because the intraseasonal component of South American rainfall varies in the 20–90-day band (Liu et al. 2023; Fernandes and Grimm 2023). Notably, the Morlet wavelet has been used to extract the flow of the Amazon, Guyana, Paraná, Orinoco, and Congo rivers (Labat et al. 2005, 2012) and the interannual-interdecadal variability in rainfall in the central Andes (Sulca et al. 2022, 2024a).

The position of the MJO along its eastward propagation is identified through the MJO real-time multivariate (RMM) index (Wheeler and Hendon 2004; hereafter WH2004). This study used the RRM index from the Bureau of Meteorology (BoM) for the period 1981-2018 (IRI 2024). Snowfall and atmospheric circulation patterns over South America at upper troposphere levels associated with the MJO are identified through composites for each pair of RMM Phases 8 + 1, 2 + 3, 4 + 5, and 6 + 7, but they are considered only when the modules of RMM1 and RMM2 are equal to or greater than 1. The statistical significance of the composites is based on Student's t test (Wilks 2011).

The E and C indices for the eastern and central equatorial Pacific SST anomalies (Takahashi et al. 2011) are used because they are poorly correlated. The E and C indices are calculated from the ERSSTv5 dataset and are freely available on the IGP website (http://met.igp.gob.pe/datos/ecindex_ersstv5.txt). The E and C indices were chosen because they do not present an intraseasonal component (Sulca et al. 2024b).

Here, neutral ENSO conditions occur when E and C are simultaneously lower, between −0.5 and +0.5. This method was chosen to avoid any effects of coastal El Niño in the results. Additionally, Central El Niño (La Niña) occurs when C is higher (lower) or equal to +1 (−1). Similarly, Eastern El Niño (La Niña) occurs when E is higher (lower) or equal to +1 (−1).

Satoh et al. (2004) reported that solid precipitation is caused by cumulonimbus clouds, which are characterised by snow in the upper parts and rainfall in the lower parts. Since cumulonimbus clouds are caused by deep convection systems, this study uses the OLR index to verify the presence of well-organised convection systems during snowfall events in the Peruvian Andes. Additionally, precipitation data are used to confirm the simultaneous occurrence of rainfall and active convection systems during snowfall events in the Peruvian Andes.

3 | Climatological Pattern of Extreme Snowfall Events in the Peruvian Andes

The climatological snowfall patterns over the Peruvian Andes from 1981 to 2018 during the DJF and JJA seasons, as simulated by the ERA5 reanalysis, are shown in Figure 1. Figure 1a shows that the ERA5 reanalysis simulates maximum snowfall over the Western and Eastern Cordilleras of the Peruvian Andes, which is twice as large along the Western Cordillera. However, the ERA5 reanalysis underestimates the intensity of the snowfall amount along the Eastern Cordillera of the central Peruvian Andes. The JJA snowfall pattern resembles the DJF snowfall pattern but is half as strong (Figure 1b).

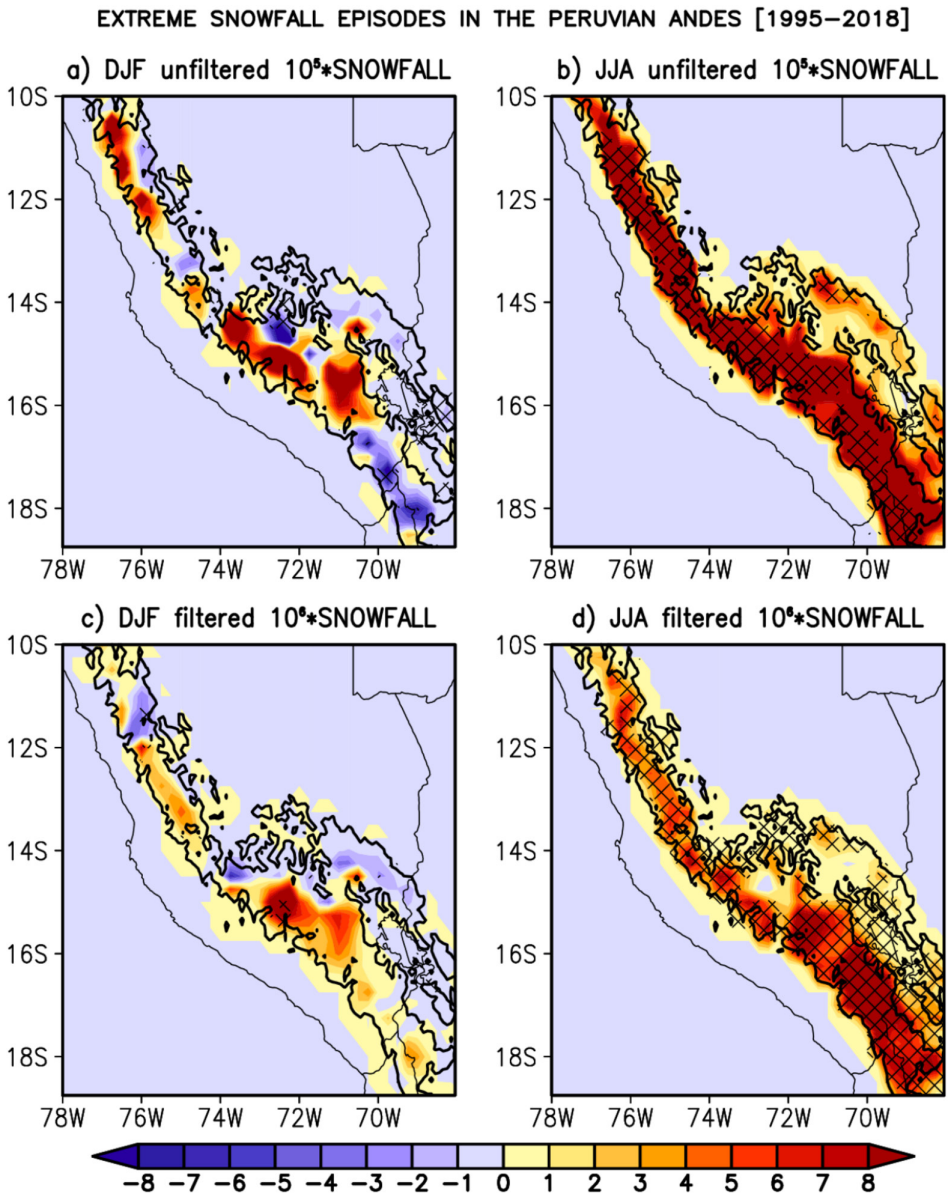

FIGURE 2 | Composites of unfiltered snowfall anomalies (in m of water) during extreme snowfall events in the Peruvian Andes during the (a) DJF and (b) JJA seasons. (c and d) As in a and b, but for filtered (20–90-day band) snowfall anomalies. The black contour represents topographic elevation above 4000 m. Hatching areas indicate significant unfiltered and filtered snowfall anomalies at the 95% confidence level. The unfiltered (filtered) snowfall anomalies were rescaled by a factor of 10^{-5} (10^{-6}). The ERA5 reanalysis data from the period from 1981 to 2016 were used in this analysis. [Colour figure can be viewed at wileyonlinelibrary.com]

The results of the composite for the unfiltered and filtered daily snow anomalies during extreme snowfall events across the Peruvian Andes in the DJF and JJA seasons are shown in Figure 2.

For the DJF season, Figure 2a–b show that unfiltered and filtered snowfall events present an increase in snowfall, although this increase is not statistically significant, over the Western Cordillera of the southern and central Peruvian Andes (north of 16.4° S). Conversely, a reduction in snowfall is observed in the remaining parts of the Peruvian Andes. The absence of significant snowfall anomalies implies that the ERA5 reanalysis is unable to simulate extreme snowfall events in the Peruvian Andes. These findings show that the current resolution of the ERA5 reanalysis is insufficient to reproduce the observed pattern of extreme snowfall events in the Peruvian Andes during the austral summer. During the JJA season, as shown in Figure 2c, unfiltered snow episodes exhibit a significant increase in snowfall over the entire Peruvian Andes, with the most substantial increases observed along the Western Cordillera and Eastern Cordillera of the Peruvian Altiplano. Conversely, there are no significant increases in snowfall over Lake Titicaca. These findings highlight the regional nature of extreme snowfall events in the Peruvian Andes during the austral winter season. Additionally, they indicate that the horizontal resolution of the ERA5 model is sufficient for capturing and reporting these extreme snowfall events in the Peruvian Andes. The pattern of filtered snowfall anomalies closely mirrors the unfiltered snow pattern, extending to cover Lake Titicaca and the Bolivian Altiplano (Figure 2d).

These findings indicate that extreme winter snowfall events in the western Andes of the Peruvian Andes exhibit an intraseasonal nature.

4 | Patterns of Snowfall and Changes in Atmospheric Circulation Over South America During the MJO Under ENSO-Neutral Conditions

4.1 | Austral Summer (DJF)

Under non-MJO conditions, Table 1 shows that 8 out of 25 extreme snowfall events in the Peruvian Andes occurred outside of active MJO phases during austral summer. This suggests that other large-scale and local forcings contribute to extreme snowfall events in this region. However, this study does not include further characterisation of these extreme snowfall events, which is beyond the scope of this research.

During RMM Phases 8 + 1, as displayed in Figure 3a, snowfall increases along the Western Cordillera of the southern Peruvian Andes. In contrast, a simultaneous reduction in snowfall is observed in the remaining Peruvian Andes. This increase in snowfall agrees with the negative velocity potential anomalies over the Pacific Basin and South America (Figure 3b). Significant negative OLR anomalies and an upper-level anticyclonic circulation centered at 65° W, 23° S (Figure 3c) suggest an enhanced and southward-displaced upper-level Bolivian high from its climatological position (Fernandes and Grimm 2023). Southeasterly VIHT anomalies originating from the southern Atlantic Ocean are observed over the Peruvian and Bolivian Amazon (Figure 4a). These anomalies indicate the intrusion of an extratropical Rossby wave into the continent along the eastern flank of the Peruvian Andes (Garreaud 1999; Fernandes and Grimm 2023), reducing moisture over the Eastern Cordillera while favouring convection over the southern Peruvian Andes at intraseasonal timescales. These circulation anomalies account for the reduction in snowfall in the Eastern Cordillera of the southern Peruvian Andes (Figure 4a). Northwesterly VIHT anomalies are present over the Western Cordillera of the southern Peruvian Andes (Figure 4a). Both southeasterly and northwesterly VIHT anomalies contribute to the southward displacement of the upper-level Bolivian High, causing wet anomalies over the southern Peruvian Andes (Figure 4b). Conversely, westerly VIHT anomalies dominate over the central and northern Peruvian Andes north of 11° S (Figure 4a), leading to dry anomalies in these regions (Figure 4b) due to the weakening of the easterly humidity flux from the Amazon Basin (Vuille et al. 2000; Segura et al. 2019). These findings suggest that the increase in snowfall in the Western Cordillera of the southern Peruvian Andes during MJO Phases 8 + 1 is dynamically linked to an enhanced upper-level Bolivian High displaced southward from its climatological position, influenced by the extratropical teleconnection via the intrusion of extratropical Rossby wave trains into the continent along the eastern flank of the Peruvian Andes. Conversely, the decrease in snowfall in the central and northern Peruvian Andes during MJO Phases 8 + 1 is dynamically linked to the weakening of the easterly moisture flux from the Amazon Basin as the MJO crosses equatorial South America.

Concerning RMM Phases 2 + 3, Figure 3d displays an increase in snowfall across the Peruvian Andes south of 10° S. The increase in snowfall corresponds to a velocity potential dipole with positive and negative anomalies over the tropical Andes and eastern Brazil (Figure 3e). This velocity potential dipole is consistent with an OLR dipole characterised by negative anomalies over the Peruvian Andes and positive OLR anomalies over northeastern Brazil. It also coincides with upper-level easterly winds over the Peruvian Andes and simultaneous northeasterly wind anomalies over northeastern Brazil at 200 hPa (Figure 3f), indicating an enhanced upper-level Bolivian High-Nordeste Low system over the continent. The enhanced upper-level BH-NL system is consistent with significant easterly VIHT anomalies and wet anomalies over the southern Peruvian Andes (Figure 4c,d). These conditions even extend toward eastern Brazil, demonstrating that the increase in snowfall results from the strengthening of the eastward moisture flux from the Amazon Basin. These results align with the circulation patterns associated with wet spells in the central Peruvian Andes caused by a strengthened upper-level BH-NL system on intraseasonal timescales (Sulca et al. 2016). Additionally, the upper-level easterly wind anomalies crossing the South American continent extend to the tropical Atlantic Ocean, suggesting that they are caused by deep convection over the Indian Ocean and the African continent (Gahtan and Roundy 2021), similar to patterns observed at interannual timescales (Lenter and Cook 1997; Chen et al. 1999). These findings indicate that the increase in snowfall in the southern Peruvian Andes during MJO Phases 2 + 3 is dynamically linked to a strengthened upper-level BH-NL system, driven by deep convection over the Indian Ocean and the African continent that intensifies upper-level easterly flow.

In RMM Phases 4 + 5, Figure 3g displays a reduction in snowfall across the Peruvian Andes. The reduction in snowfall corresponds to a positive velocity potential over South America and the tropical Atlantic Ocean (Figure 3h). This positive velocity potential is linked to slightly positive OLR anomalies over the Peruvian Andes. Upper-level westerly wind anomalies over the southern Peruvian Andes and a positive core of geopotential height anomalies over the southern coast of Peru, centered at 31° S, 75° W at 200 hPa (Figure 3i), suggest that the reduction in snowfall in the Peruvian Andes is driven by the westward dry air flux from the Pacific Ocean (Garreaud 1999). This observation aligns westerly VIHT anomalies and dry anomalies over the Western Cordillera of the southern Peruvian Andes (Figure 4e,f). Figure 4e,f also illustrate significant easterly VIHT anomalies and wet anomalies over the Eastern Cordillera of the southern Peruvian Andes. These conditions contradict the reduction in snowfall over the Eastern Cordillera of the southern Peruvian Andes, suggesting that ERA5 reanalysis cannot capture the increase in snowfall in this region during MJO Phases 4 + 5 in austral summer. Figure 3i also shows an upper-level anticyclonic circulation over the southern part of the South Atlantic Ocean, representing the extratropical teleconnection of MJO Phase 4 (Fernandes and Grimm 2023), which weakens the upper-level Bolivian High. These findings indicate that the reduction in snowfall in the Peruvian Andes during MJO Phases 4 + 5 is dynamically linked to a weakening of the upper-level Bolivian High, driven by the equatorward propagation of an extratropical Rossby wave along the eastern coast of South America.

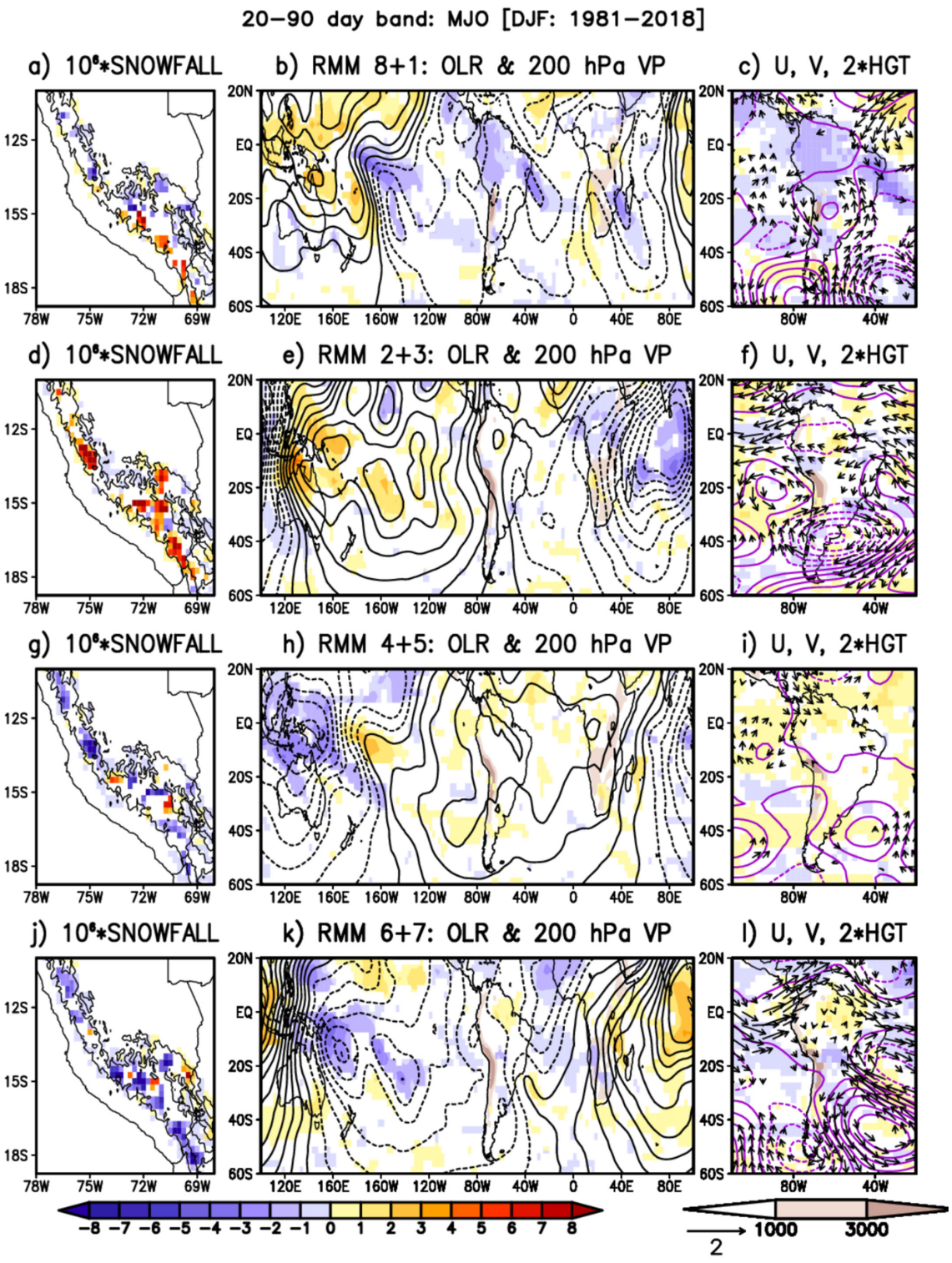

FIGURE 3 | Composite of filtered anomalies in the 20–90-day band for (a) snowfall (m of water) and (b) OLR ($W\,m^{-2}$) and velocity potential ($m^2\,s^{-1}$) and (c) OLR ($W\,m^{-2}$), wind ($m\,s^{-1}$) and geopotential height (m) over the Southern Hemisphere at 200 hPa for RMM Phases 8 + 1 under neutral ENSO conditions during austral summer (December–January–February, DJF). (d–f) As in (a–c) but for RMM Phases 2 + 3. (g–i) As in (a–c) but for RMM Phases 4 + 5. (j–l) As in (a–c) but for RMM Phases 6 + 7. Only wind anomalies statistically significant at the 95% confidence level are shown. Shaded areas indicate significant anomalies of snowfall and OLR at the 95% confidence level. The black contour represents topographic elevation above 4000 m. The black contour represents topographic elevation above 4000 m. The filtered (unfiltered) snowfall anomalies were rescaled by a factor of 10^{-6} (10^{-5}). The geopotential height anomalies were rescaled by a factor of 2. The ERA5 reanalysis data from the period from 1981 to 2018 were used in this analysis. [Colour figure can be viewed at wileyonlinelibrary.com]

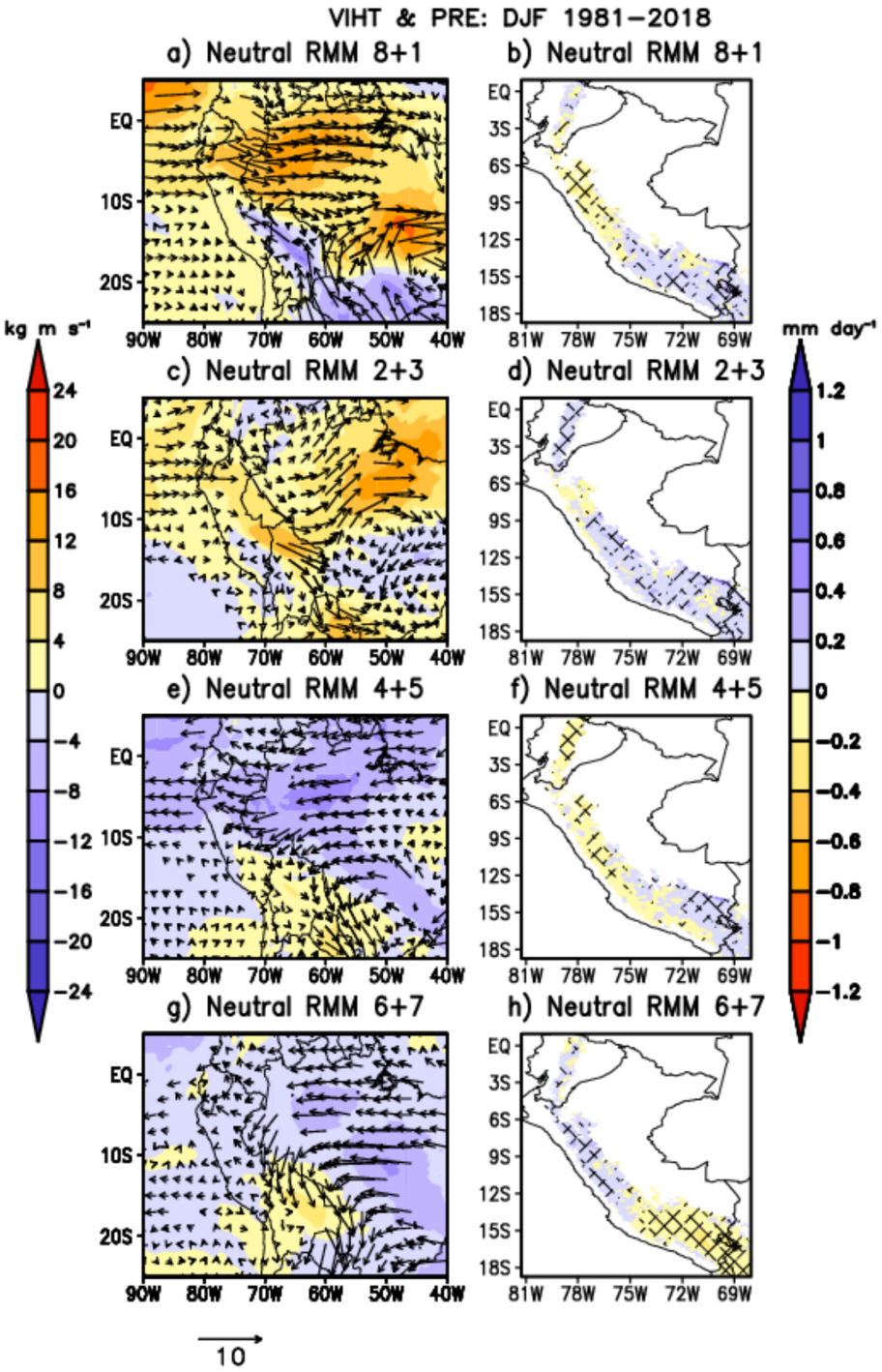

FIGURE 4 | Composite of filtered anomalies in the 20–90-day band for (a) vertically integrated humidity transport ($kg\,m^{-1}\,s^{-1}$) and (b) precipitation ($mm\,day^{-1}$) during MJO Phases 8 + 1 under non-ENSO conditions during austral summer (December–January–February, DJF). The black vectors represent VIHT anomalies that are statistically significant at the 95% confidence level. Hatched areas indicate significant precipitation anomalies (> 2500 m) at the 95% confidence level. The PISCOp v2.1 and the ERA5 reanalysis datasets of the period from 1981 to 2018 were used in this analysis. (c and d) As in (a and b) but for MJO Phases 2 + 3. (e and f) As in (a and b) but for MJO Phases 4 + 5. (g and h) As in (a and b) but for MJO Phases 6 + 7. [Colour figure can be viewed at wileyonlinelibrary.com]

Regarding RMM Phases 6 + 7, Figure 3j illustrates a decrease in snowfall across the central and southern Peruvian Andes. Negative velocity potential anomalies are evident over the Pacific Basin and South America (Figure 3k). However, non-significant positive OLR anomalies and significant upper-level westerly winds over the Peruvian Andes at 200 hPa (Figure 3l) indicate a weakening of the upper-level Bolivian high. These results agree with slight southeasterly VIHT anomalies and dry anomalies over the southern Peruvian Andes (Figure 4g,h). Figure 3l also shows an upper-level anticyclonic circulation over the southern portion of the South Atlantic Ocean, indicating that the equatorward propagation of the extratropical Rossby wave trains along the eastern coast of Brazil, which weakens the upper-level BH-NL system (Chen

et al. 1999). These findings indicate that the decrease in snowfall in the southern Peruvian Andes during MJO Phases 6 + 7 is due to the reduced easterly moisture flux from the Amazon Basin, driven by the weakening of the upper-level BH-NL system over South America, which is caused by the eastward propagation of extratropical Rossby wave trains along the eastern coast of Brazil.

4.2 | Austral Winter (JJA)

Under non-MJO conditions, Table 1 shows that 9 out of 35 extreme snowfall events in the Peruvian Andes occurred outside of active MJO phases during austral winter. This suggests that other large-scale and local forcings contribute to extreme snowfall events in this region. However, this study does not include further characterisation of these extreme snowfall events, which is beyond the scope of this research.

During RMM Phases 8 + 1, negative snowfall anomalies are observed over the Western Cordillera of the southern Peruvian Andes (Figure 5a). Figure 5b,c display nonsignificant negative OLR anomalies and negative velocity potential anomalies over the southern Peruvian Andes. Significant upper-level easterly wind anomalies, which are part of an upper-level ridge, are observed over the southern Peruvian Andes at 200 hPa. These easterly wind anomalies are part of an upper-level extratropical Rossby wave train that crosses the northern Andes of Chile and Peru near 67° W, 19° S (Figure 5c). This explains the observed northwesterly VIHT anomalies and dry anomalies over the Western Cordillera of the southern Peruvian Andes (Figure 6a,b). These results indicate that the transport of dry air masses from the Pacific Ocean toward the Peruvian Andes suppressed snowfall in these areas during MJO Phases 8 + 1. Based on these findings, extreme snowfall events 4–8 (Table 1) cannot be attributed to the effect of MJO Phase 8 because its respective circulation patterns inhibit snowfall in the Peruvian Andes (Figure 5a).

During RMM Phases 2 + 3, as shown in Figure 5d, snowfall anomalies decrease in the Peruvian Andes. This is consistent with positive anomalies in OLR and velocity potential (Figure 5e). Significant upper-level easterly wind anomalies associated with an upper-level ridge are observed over the northern Argentinian Andes near 65° W, 30° S (Figure 5f). This aligns with southeasterly VIHT anomalies and dry anomalies over the Eastern Cordillera of the southern Peruvian Andes (Figure 6c,d). These circulation anomalies suggest that the transport of dry air masses from the Pacific Ocean toward the southern Peruvian Andes suppresses snowfall in this region. Additionally, Figure 5e illustrates the equatorward propagation of an extratropical Rossby wave train crossing the Altiplano region and moving northward toward the northern Argentinian Andes (65° W, 28° S). Thus, during the MJO under RMM Phases 2 + 3, snowfall decreases over the southern Peruvian Andes due to the equatorward propagation of an extratropical Rossby wave train crossing the Altiplano region during the austral winter on intraseasonal timescales.

During RMM Phases 4 + 5, as shown in Figure 5g, negative snowfall anomalies occur in the central Peruvian Andes and the Eastern Cordillera of the southern Peruvian Andes, whereas snowfall increases in the Western Cordillera of the southern Peruvian Andes. The reduction in snowfall in the central Peruvian Andes is in agreement with nonsignificant positive OLR anomalies and nonsignificant upper-level westerly wind anomalies over the central Peruvian Andes at 200 hPa (Figure 5h,i). This suggests a reduction in rainfall and easterly moisture flux from the Amazon (Figure 6e,f). The increase in snowfall in the Western Cordillera of the southern Peruvian Andes corresponds to either negative but not significant OLR anomalies or positive velocity potential anomalies (Figure 5h,i). Significant upper-level northeasterly wind anomalies are observed over the southern Peruvian Andes, forming part of an upper-level ridge over the coast of central Brazil at 200 hPa (45° W, 30° S) (Figure 5i). This pattern is consistent with northeasterly VIHT anomalies and wet anomalies over the Altiplano region (Figure 6e,f). These circulation anomalies suggest enhanced moisture transport from the Amazon Basin to the southern Peruvian Andes, favouring snowfall in the Western Cordillera over the southern Peruvian Andes. Despite wet conditions across the southern Peruvian Andes, the Eastern Cordillera shows negative snowfall anomalies (Figure 5g), suggesting that the ERA5 reanalysis fails to accurately reproduce snowfall in this region. Additionally, Figure 5i shows that the upper-level ridge is part of extratropical Rossby waves propagating toward lower latitudes along the eastern coast of Brazil. Thus, during MJO Phases 4 + 5, a snowfall dipole emerges with increased snowfall over the southern Peruvian Andes and reduced snowfall in the central Peruvian Andes, driven by upper-level westerly and northeasterly wind anomalies. The decrease in snowfall in the central Peruvian Andes is caused by weakened moisture flux from the east, driven by upper-level westerly wind anomalies over this region associated with the eastward propagation of the MJO. The increase in snowfall in the Western Cordillera of the southern Peruvian Andes is caused by strengthened moisture flux from the east, driven by the equatorward propagation of an extratropical Rossby wave train along the coast of Brazil on intraseasonal timescales. Based on these findings, extreme snowfall events 27–31 (Table 1) were likely caused by increased moisture flux from the east and strong organisation of convection over the Peruvian Andes during MJO Phase 5.

During RMM Phases 6 + 7, positive snowfall anomalies occur across the entire Peruvian Andes (Figure 5j). Figure 5k shows significant negative anomalies of OLR and velocity potential across the entire Peruvian Andes. Significant upper-level westerly wind anomalies are observed over the Peruvian Andes at 200 hPa (Figure 5l). These upper-level westerly wind anomalies are part of an upper-level trough located in the northern Andes of Chile and Peru at 67° W, 19° S. This explains the non-significant northeasterly VIHT anomalies are observed along the eastern flank of the Peruvian Andes and significant wet anomalies across the Peruvian Andes (Figure 6g,h). These results indicate that strengthened moisture flux from the east triggers snowfall across the entire Peruvian Andes during MJO Phases 6 + 7 in the austral winter. This same mechanism works for the extreme precipitation over the southern Peru during the JJA season (Segura et al. 2022). Figure 5l also shows extratropical Rossby wave trains propagating toward low latitudes, crossing the Altiplano region. Thus, during MJO Phases 6 + 7, snowfall increases

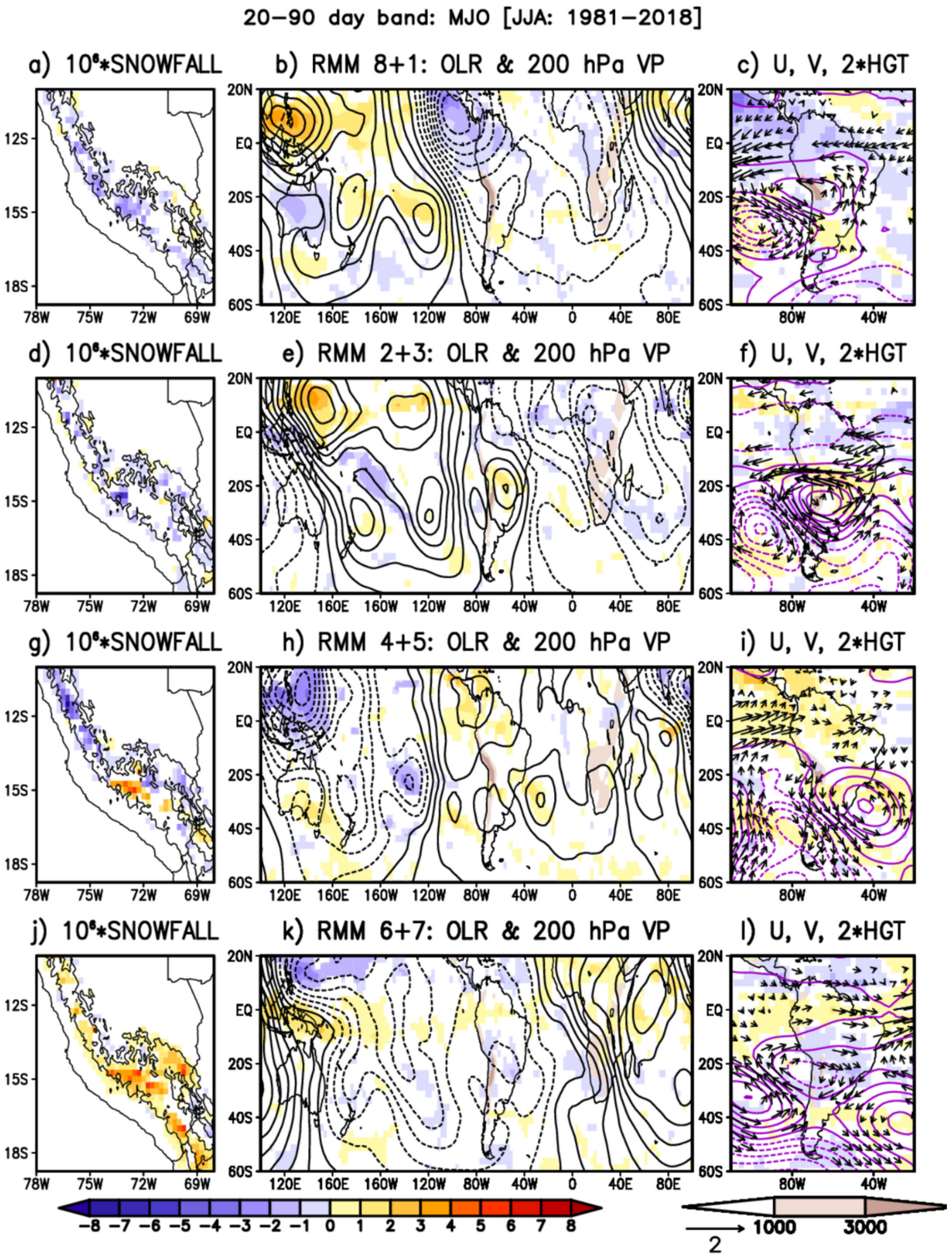

FIGURE 5 | Composite of filtered anomalies in the 20–90-day band for (a) snowfall (m of water) and (b) OLR ($W m^{-2}$) and velocity potential ($m^2 s^{-1}$) and (c) OLR ($W m^{-2}$), wind ($m s^{-1}$) and geopotential height (m) over the Southern Hemisphere at 200 hPa for RMM Phases 8 + 1 under neutral ENSO conditions during austral winter (June–July August, JJA). (d–f) As in (a–c) but for RMM Phases 2 + 3. (g–i) As in (a–c) but for RMM Phases 4 + 5. (j–l) As in (a–c) but for RMM Phases 6 + 7. Only wind anomalies statistically significant at the 95% confidence level are shown. The shaded areas indicate significant snowfall and OLR anomalies at the 95% confidence level. The black contour represents the topographic elevation above 4000 m. The filtered (unfiltered) snowfall anomalies were rescaled by a factor of 10^{-6} (10^{-5}). The geopotential height anomalies were rescaled by a factor of 2. The ERA5 reanalysis data from the period from 1981 to 2018 were used in this analysis. [Colour figure can be viewed at wileyonlinelibrary.com]

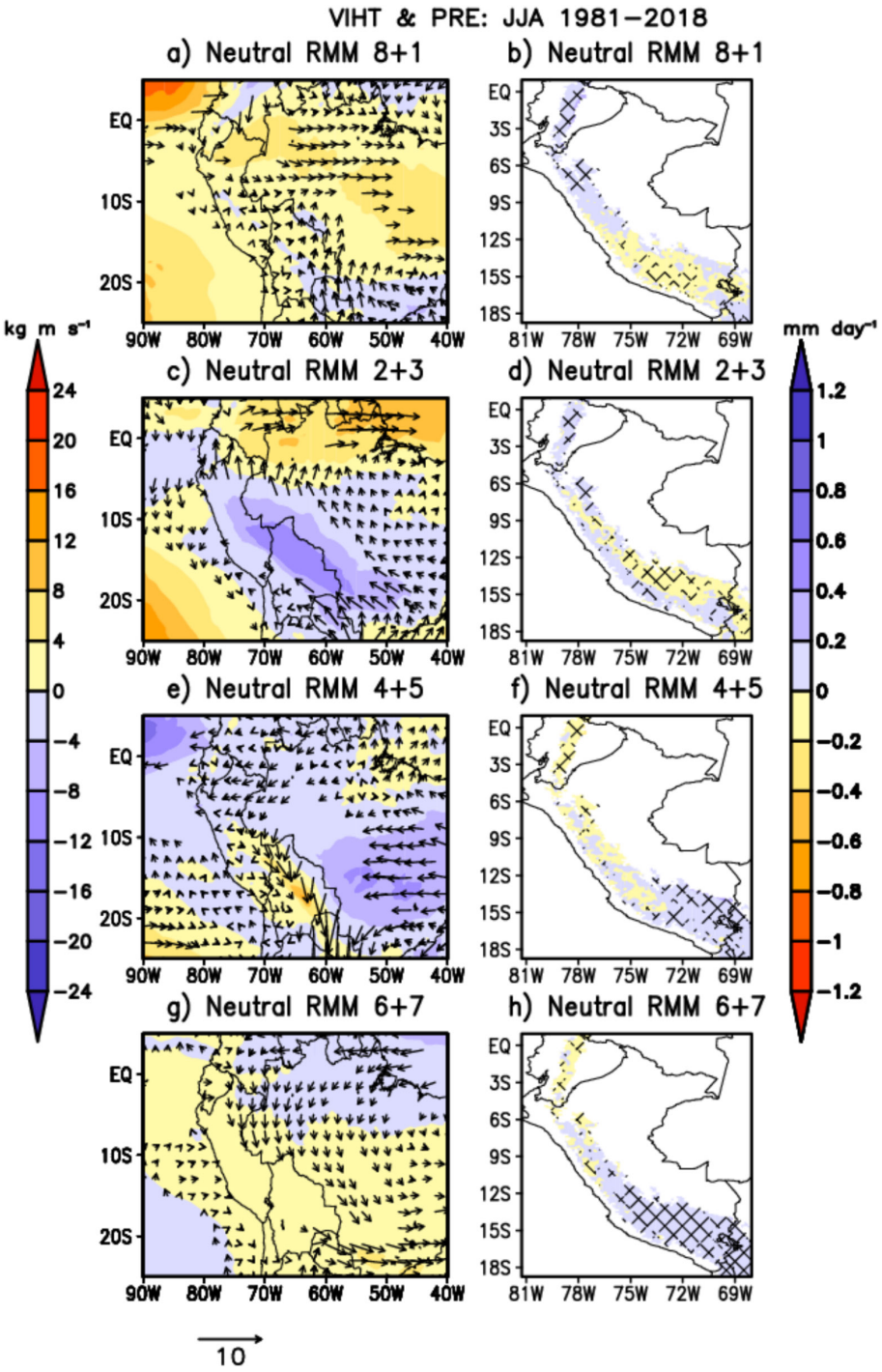

FIGURE 6 | Composite of filtered anomalies in the 20–90-day band for (a) vertically integrated humidity transport ($kg\,m^{-1}\,s^{-1}$) and (b) precipitation ($mm\,day^{-1}$) during MJO Phases 8 + 1 under non-ENSO conditions during austral winter (June–July August, JJA). The black vectors represent VIHT anomalies that are statistically significant at the 95% confidence level. Hatched areas indicate significant precipitation anomalies (> 2500 m) at the 95% confidence level. The PISCOp v2.1 and the ERA5 reanalysis datasets of the period from 1981 to 2018 were used in this analysis. (c and d) As in (a and b) but for MJO Phases 2 + 3. (e and f) As in (a and b) but for MJO Phases 4 + 5. (g and h) As in (a and b) but for MJO Phases 6 + 7. [Colour figure can be viewed at wileyonlinelibrary.com]

across the entire Peruvian Andes because strengthened moisture from the east driven by extratropical Rossby wave trains propagates toward low latitudes, crossing the Altiplano region. Based on these findings, extreme snowfall events 4 and 32–35 (Table 1) were likely caused by enhanced moisture flux from the east and a strong organisation of convection over the Peruvian Andes during MJO Phases 6 + 7.

5 | Modulation Effect of ENSO Diversity on MJO Impacts on Snowfall in the Peruvian Andes During Austral Summer

The results of the composites for the 20–90-day bands of snowfall, precipitation, OLR and vertically integrated moisture transport anomalies during active MJO under Central El Niño,

Central La Niña, Eastern El Niño, and Eastern La Niña during the DJF season from 1981 to 2018 are shown in Figures 7–11.

5.1 | Central El Niño

With respect to Central El Niño, MJO Phases 8 + 1 and 6 + 7 lead to a reduction in snow in the Peruvian Andes (Figure 7a–d). Conversely, the MJO Phases 2 + 3 and 4 + 5 are associated with increased snowfall in the Western Cordillera of the Peruvian Andes and simultaneously decreased snowfall over the Eastern Cordillera in the southern Peruvian Andes (Figure 7b,c). This increase in snowfall corresponds to significant wet anomalies observed in the western and central Peruvian Andes (Figure 8c). However, these same regions do not exhibit significant negative OLR anomalies (Figure 9c), suggesting that the snowfall increase is not linked to a well-defined convection system. Additionally, Figure 10b,c depict upper-level easterly wind anomalies over the Peruvian Andes, which are associated with the strengthening of the upper-level BH-NL system (Figure 10b,c) but are not statistically significant during RMM Phases 4 + 5. This implies that upper-level easterly flow anomalies over South America, which drive deep convection over the Indian Ocean and the African continent, dominate the upper-level westerly flow anomalies over SA, which drive warm SST anomalies in the central Pacific Ocean. Based on these findings, the extreme snowfall event on January 23, 2004 (event 3, Table 1), was likely caused by enhanced moisture flux from the east and a strong organisation of convection over the Peruvian Andes during MJO Phases 2 + 3, influenced by Central El Niño.

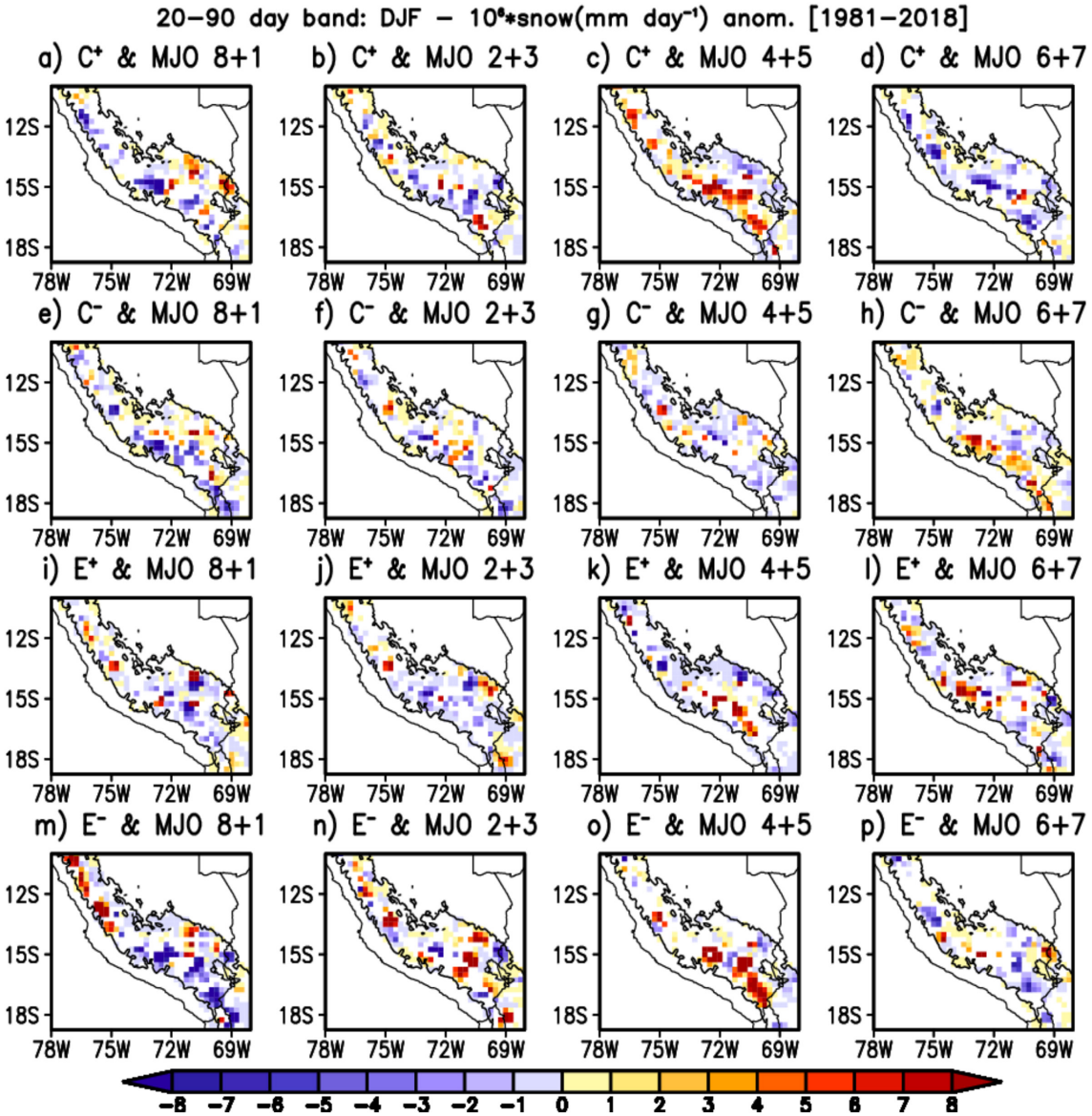

FIGURE 7 | Composite of filtered anomalies in the 20–90-day band for snowfall (m of water) over the Peruvian Andes for (a) RMM Phases 8 + 1, (b) RMM Phases 2 + 3, (c) RMM Phases 4 + 5, and (d) RMM Phases 6 + 7 under Central El Niño during austral summer (December–January–February, DJF). (e–h) As in (a–d) but for Central La Niña. (i–l) As in (a–d) but for Eastern El Niño. (m–p) As in (a–d) but for the Eastern La Niña. The shaded areas indicate significant snowfall anomalies at the 90% confidence level. The black contour represents the topographic elevation above 2500 m. The filtered snowfall anomalies were rescaled by a factor of 10^{-6}. The analysis is based on the period from 1981 to 2018. [Colour figure can be viewed at wileyonlinelibrary.com]

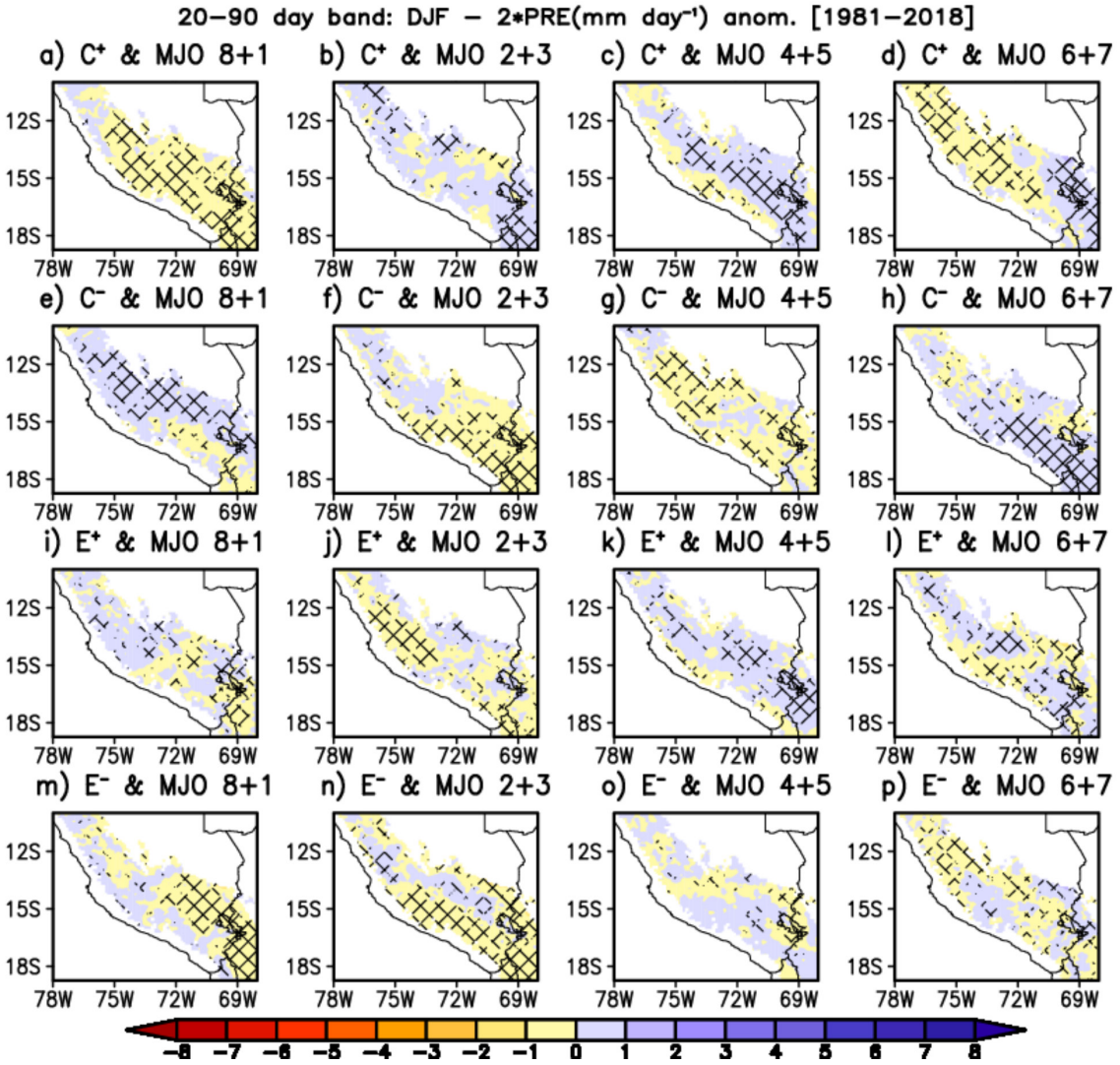

FIGURE 8 | Composite of filtered anomalies in the 20–90-day band for precipitation (mm day^{-1}) over the Peruvian Andes for (a) RMM Phases 8 + 1, (b) RMM Phases 2 + 3, (c) RMM Phases 4 + 5, and (d) RMM Phases 6 + 7 under the Central El Niño during austral summer (December–January–February, DJF). (e–h) As in (a–d) but for Central La Niña. (i–l) As in (a–d) but for Eastern El Niño. (m–p) As in (a–d) but for the Eastern La Niña. The shaded areas indicate significant precipitation anomalies at the 90% confidence level. The black contour represents the topographic elevation above 2500 m. The analysis is based on the period of 1981–2018. [Colour figure can be viewed at wileyonlinelibrary.com]

5.2 | Central La Niña

During Central La Niña, MJO Phases 8 + 1, 2 + 3, and 4 + 5 reduce snowfall over the Peruvian Andes (Figure 7e–g). These reductions in snowfall agree with significant dry anomalies (Figure 8f,g) and significant positive OLR anomalies over the Peruvian Andes (Figure 9e–g). In contrast, during MJO Phases 6 + 7, snowfall increases along the Western Cordillera of the Peruvian Andes (Figure 7h). These increases in snowfall correspond to significant wet anomalies and significant negative OLR anomalies over the Western Cordillera of the southern Peruvian Andes (Figures 8h and 9h). Significant northeasterly wind anomalies over the southern Peruvian Andes result from the interaction between an upper-level cyclonic circulation anomaly over the Peruvian Pacific coast and an upper-level anticyclonic circulation anomaly over the northern Chilean Andes (68° W, 30° S) at 200 hPa (Figure 10h). These circulation patterns align with southeasterly VIHT anomalies along the eastern flank of the Peruvian Andes and westerly VIHT anomalies over the central Peruvian Andes, extending toward northeastern Brazil (Figure 11h). These southeasterly VIHT anomalies suggest a reversal of the SALLJ and the equatorward propagation of a cold surge along the eastern slope of the northern Chilean Andes. This pattern is consistent with snowfall events on the Quelccaya Ice Cap triggered by cold surges (Hardy et al. 2015). This upper-level anticyclonic circulation indicates a southward shift of the Bolivian High, driven by the intrusion of the upper-level extratropical Rossby wave train into the Altiplano region. Cold SST anomalies over the central Pacific Ocean weaken upper-level convergence over the subtropics (Webster and Holton 1982; Ferranti et al. 1990; Barreiro 2016), facilitating the penetration of an upper-level extratropical Rossby wave train into the continent, crossing the Altiplano region. These findings show that the combined effects of Central La Niña and MJO Phases 6 + 7 induce snowfall over the Western Cordillera of the southern Peruvian Andes during the austral summer by enhancing the humidity flux from the east, driven by the southward shift of the

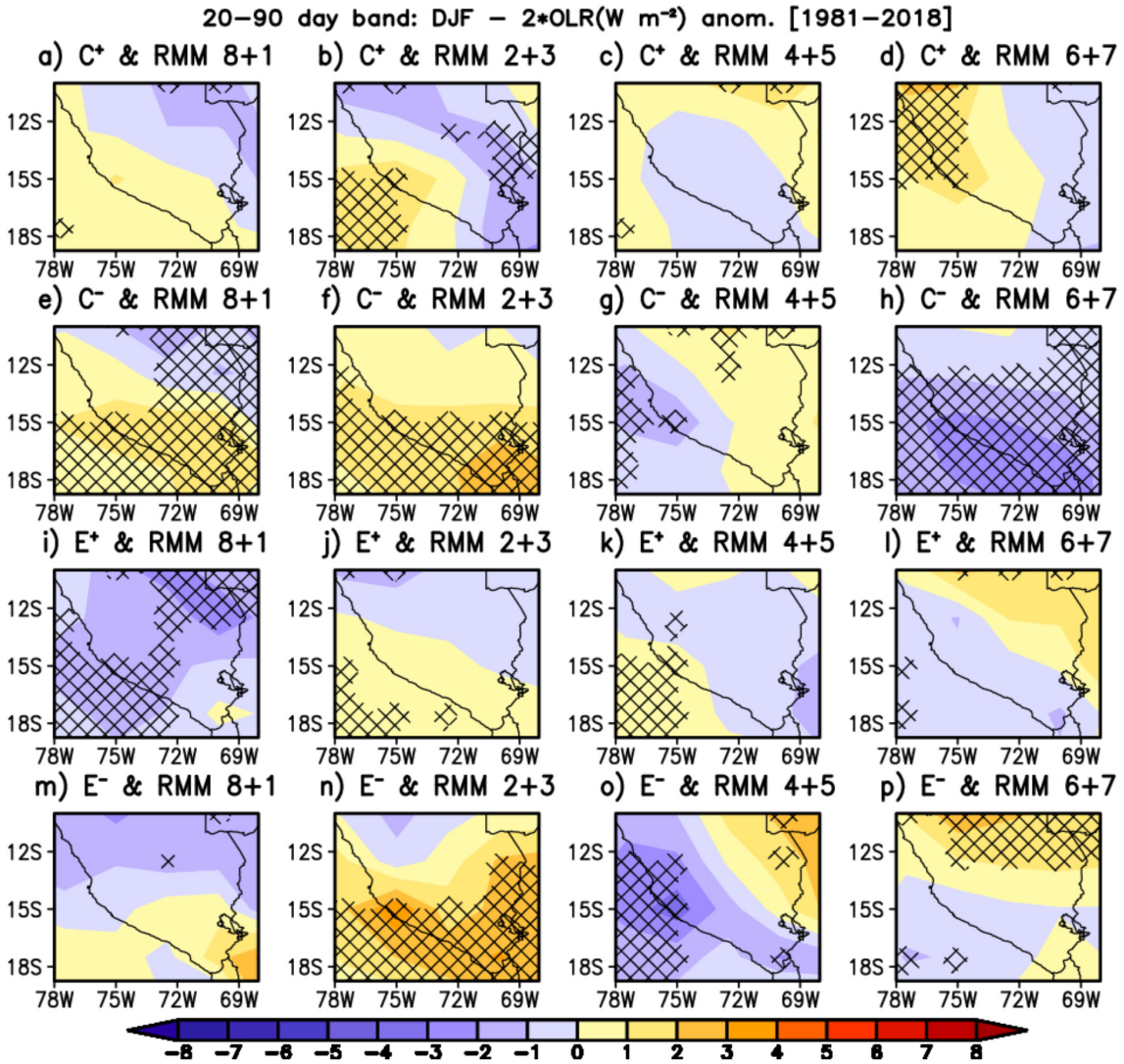

FIGURE 9 | Composite of filtered anomalies in the 20–90-day band for outgoing longwave radiation (OLR, $W m^{-2}$) over the Peruvian Andes for (a) RMM Phases 8+1, (b) RMM Phases 2+3, (c) RMM Phases 4+5, and (d) RMM Phases 6+7 under Central El Niño during austral summer (December–January–February, DJF). (e–h) As in (a–d) but for Central La Niña. (i–l) As in (a–d) but for Eastern El Niño. (m–p) As in (a–d) but for the Eastern La Niña. The shaded areas indicate significant OLR anomalies at the 90% confidence level. The black contour represents the topographic elevation above 2500 m. The analysis is based on the period from 1981 to 2018. [Colour figure can be viewed at wileyonlinelibrary.com]

Bolivian High in response to the equatorial propagation of an upper-level extratropical Rossby wave train into the continent, crossing the Altiplano region. Based on these findings, extreme snowfall events 15–17 (Table 1) were likely caused by enhanced moisture flux from the east and a strong organisation of convection over the Peruvian Andes during MJO Phases 6+7, influenced by Central La Niña. Conversely, extreme snowfall events 2, 9–12, and 18–20 cannot be attributed to the combined effects of Central La Niña and MJO Phases 8+1, 2+3 and 4+5 because their respective circulation patterns inhibit snowfall in the Peruvian Andes (Figure 7e–g).

5.3 | Eastern El Niño

With respect to Eastern El Niño, MJO Phases 8+1 and 2+3 reduce snowfall in the Peruvian Andes (Figure 7i,j). Conversely, MJO Phases 4+5 and 6+7 cause positive snowfall anomalies over the western and central parts of the Peruvian Andes while simultaneously reducing snowfall in the Eastern Cordillera of southern Peru (Figure 7k,l). This increase in snowfall aligns with the observed wet anomalies in the central and eastern parts of the Peruvian Andes and even extends toward the Bolivian Altiplano (Figure 8k,l). However, these regions exhibit nonsignificant negative OLR anomalies over the southern Peruvian Andes (Figure 9k,l), indicating a lack of organised convection systems in this region. There are significant easterly wind anomalies over the southern Peruvian Andes and significant northerly wind anomalies over the northeastern Peruvian Andes at 200 hPa, indicating a strengthened BH-NL system (Figure 10k,l). The strengthening of the BH-NL system is associated with the equatorward propagation of the extratropical Rossby wave train along the eastern coast of South America. This circulation pattern explains the predominance of easterly VIHT anomalies over the Peruvian Andes, indicating an enhanced humidity flux from the east

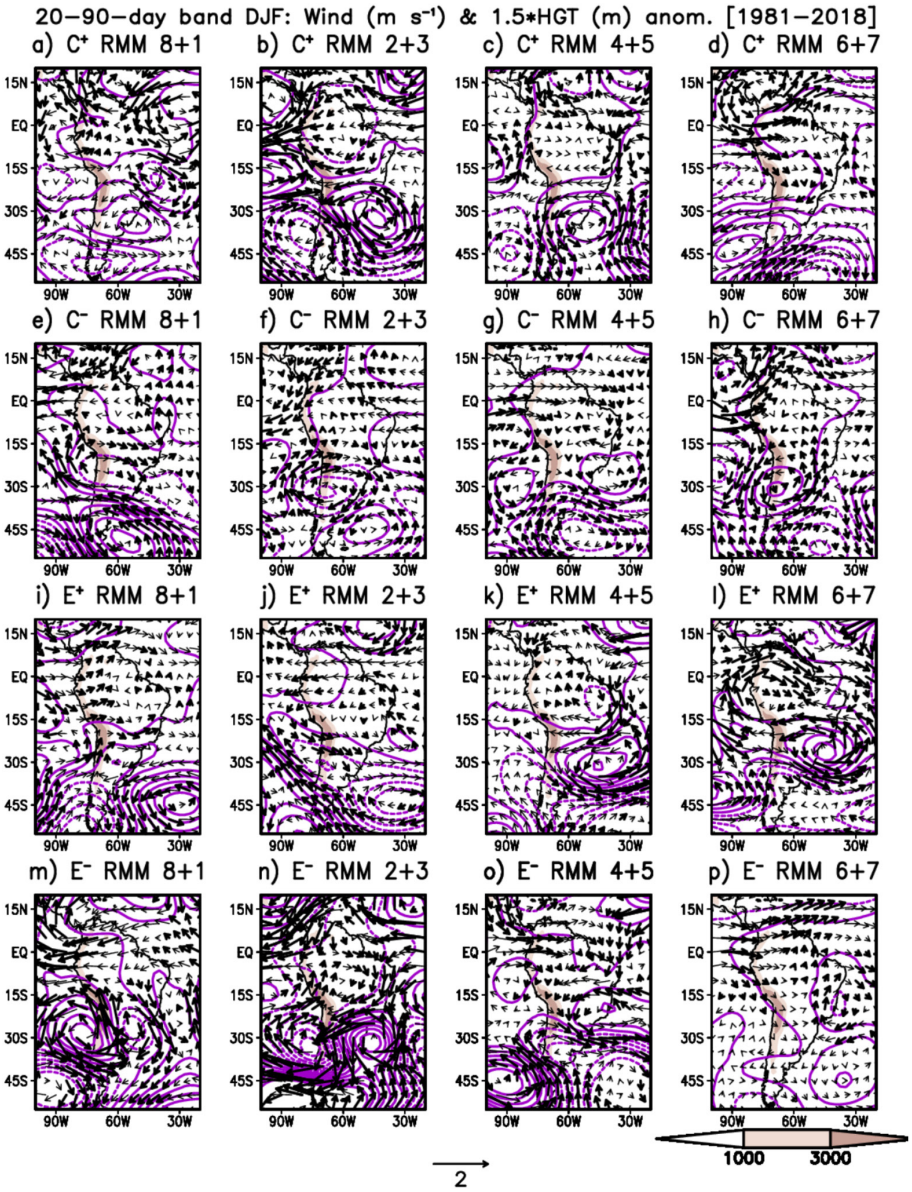

FIGURE 10 | Composite of filtered anomalies in the 20–90-day band for wind ($m\,s^{-1}$) and geopotential height (in m) anomalies over South America at 200 hPa for RMM Phases 8 + 1 under (a) Central El Niño, (e) Central La Niña, (i) Eastern El Niño and (m) Eastern La Niña during austral summer (December–January–February, DJF). (b, f, j and f) As in (a, e, i and m) but for RMM Phases 2 + 3. (c, g, k and o) As in (a, e, i and m) but for RMM Phases 4 + 5. (d, h, l and p) As in (a, e, i and m) but for RMM Phases 6 + 7. Only wind anomalies statistically significant at the 95% confidence level are shown. The shaded areas indicate significant OLR ($W\,m^{-2}$) anomalies at the 95% confidence level. The grey shading represents the topographic elevation above 1000 m. The geopotential height anomalies were rescaled by a factor of 2. The ERA5 reanalysis data from the period from 1981 to 2018 were used in this analysis. [Colour figure can be viewed at wileyonlinelibrary.com]

(Figure 11k,l). Therefore, the combined effect of Eastern El Niño and MJO Phases 4 + 5 and 6 + 7 induces snowfall over the Western Cordillera of the southern Peruvian Andes. This occurs through a strengthened moisture flux from the east, driven by an enhanced upper-level BH-NL system over South America by the equatorward propagation of the extratropical Rossby wave train along the eastern coast of South America during austral summer. However, no extreme snowfall events occur in the Peruvian Andes during MJO Phases 4 + 5 under Eastern El Niño (Table 1). This suggests that the primary limiting factor of a strongly organised convection system over the Peruvian Andes.

5.4 | Eastern La Niña

Under Eastern La Niña conditions, MJO Phases 8 + 1 and 6 + 7 are associated with reduced snowfall over the Western Cordillera of the southern Peruvian Andes (Figure 7m,p). However, wet anomalies are observed over the Western Cordillera of the southern Peruvian Andes in the same MJO Phases (Figure 8m,p). Positive OLR anomalies occur over the Western Cordillera of the southern Peruvian Andes, but they are not statistically significant (Figure 9m,p). Additionally, MJO Phases 2 + 3 produce mixed snowfall anomalies across most of the Peruvian Andes (Figure 7n). These same MJO Phases induce significant dry anomalies over the southern

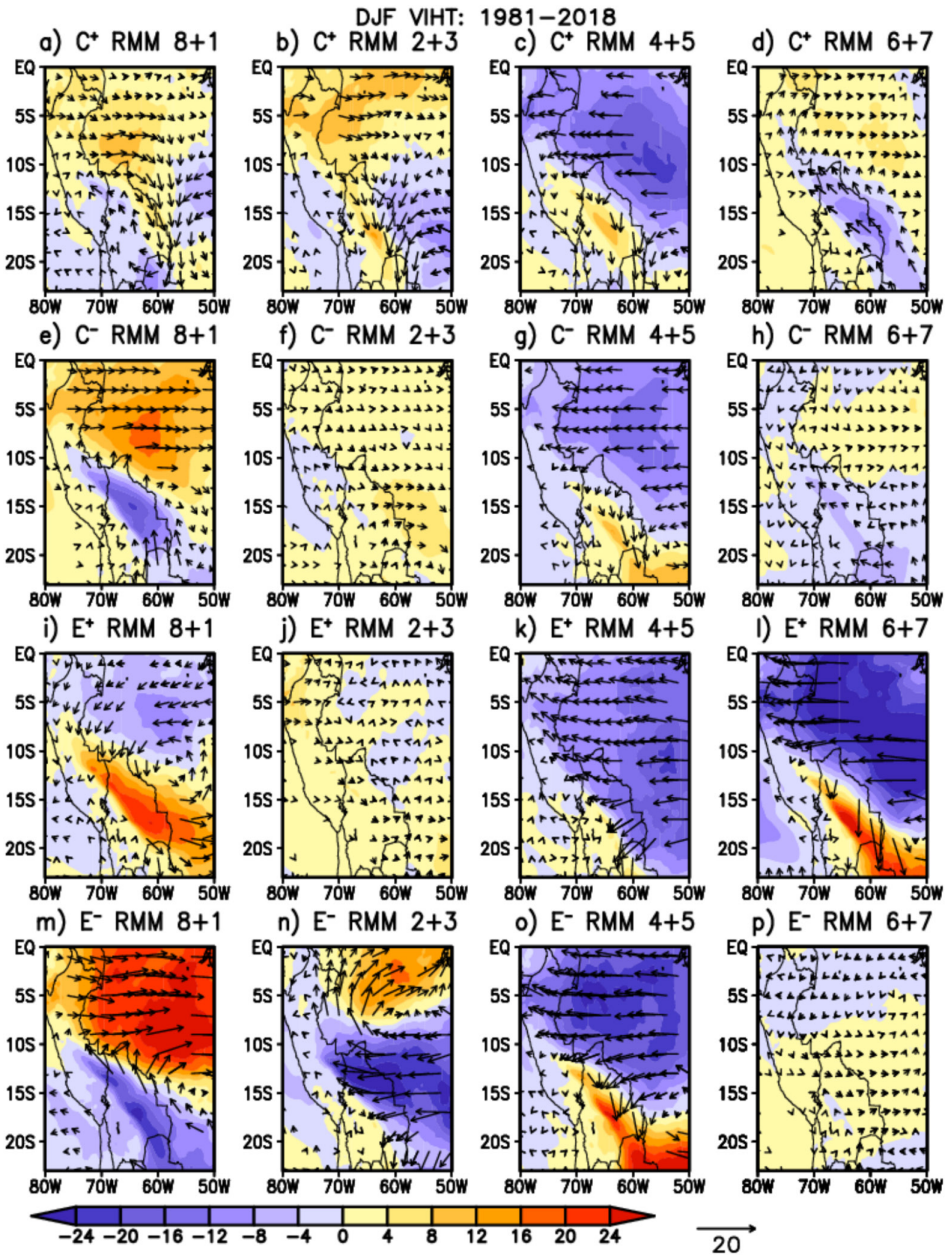

FIGURE 11 | Composite of filtered anomalies in the 20–90-day band for vertically integrated humidity transport (VIHT, kg $m^{-1}s^{-1}$) over the Peruvian Andes under Central El Niño conditions during austral summer (December–January–February, DJF) for (a) RMM Phases 8 + 1, (b) RMM Phases 2 + 3, c) RMM Phases 4 + 5, and (d) RMM Phases 6 + 7. (e–h) As in (a–d) but for Central La Niña. (i–l) As in (a-d) but for Eastern El Niño. (m–p) As in (a–d) but for the Eastern La Niña. The shaded areas represent the easterly component of vertically integrated humidity transport. The black vectors are statistically significant at the 95% confidence level. The analysis is based on the period from 1981 to 2018. The ERA5 reanalysis was used in this analysis. [Colour figure can be viewed at wileyonlinelibrary.com]

Peruvian Andes (Figure 8n). The inconsistency between snowfall and precipitation patterns over the Peruvian Andes suggests that the ERA5 reanalysis struggles to accurately simulate positive snowfall anomalies. In contrast, MJO Phases 4 + 5 are associated with increased snowfall over the Western Cordillera of the southern Peruvian Andes (Figure 7o). The positive snowfall anomalies are in agreement with the wet anomalies observed over the Western Cordillera of the southern Peruvian Andes, although they are not statistically significant (Figure 8o). However, the southern Peruvian Andes exhibit negative OLR anomalies, although these anomalies are not statistically significant (Figure 9o). Significant northeasterly wind anomalies are observed over the southern Peruvian Andes at 200 hPa (Figure 10o). These northeasterly wind anomalies are part of an extratropical Rossby wave train propagating along the coast of Brazil at 200 hPa. These circulation anomalies explain the easterly VIHT anomalies over the study region and throughout Brazil (Figure 11o), indicating that increased snowfall over the Western Cordillera in the southern Peruvian Andes is driven by enhanced moisture flux from the Amazon Basin. These circulation patterns indicate that the ERA5 reanalysis fails to reproduce the increased snowfall over the Eastern Cordillera in the southern Peruvian Andes. Therefore, the combined effect of Eastern La Niña and MJO Phases 4 + 5 leads to increased snowfall over the southern Peruvian Andes during the DJF season.

However, no extreme snowfall events are observed in the Peruvian Andes during MJO Phases 4+5 under Eastern El Niña alone (event 4 in Table 1). This suggests that the absence of a strongly organised convection system over the southern Peruvian Andes is the primary limiting factor.

6 | Modulation Effect of ENSO Diversity on MJO Impacts on Snowfall in the Peruvian Andes During Austral Winter

The results of the composites for the 20–90-day bands of snowfall, precipitation, and OLR anomalies during active MJO under Central El Niño, Central La Niña, Eastern El Niño, and Eastern La Niña during the JJA season from 1981 to 2018 are shown in Figures 12–15.

6.1 | Central El Niño

With respect to Central El Niño, MJO Phases 2+3, 4+5 and 6+7 result in a reduction in snowfall in the Peruvian Andes (Figure 12b–d). Conversely, the MJO Phases 8+1 are associated with increased snowfall in the southern Peruvian Andes, while snowfall decreases in the central Peruvian Andes (Figure 12a). This increase in snowfall coincides with significant wet anomalies observed in the southern Peruvian Andes (Figure 13a). However, these same regions exhibit both significant and slight positive OLR anomalies (Figure 14a), suggesting that the snowfall increase is linked to a localised and well-defined convection system. Additionally, Figure 15a shows upper-level easterly wind anomalies over the southern Peruvian Andes at 200 hPa, which enhance moisture flux from the east and contribute to the development of a well-defined convection system over the southern Peruvian Andes, leading to snowfall. Figure 15a also shows that the upper-level easterly wind anomalies are part of the equatorward propagation of an extratropical Rossby wave train along the eastern coast of Brazil at 200 hPa. Based on these findings, the extreme snowfall events of August 9–10, 2004 (events 9 and 10, Table 1), were likely caused by enhanced moisture flux from the east and a strong organisation of convection over the Peruvian Andes during MJO Phases 8+1 in the JJA season, influenced by Central El Niño.

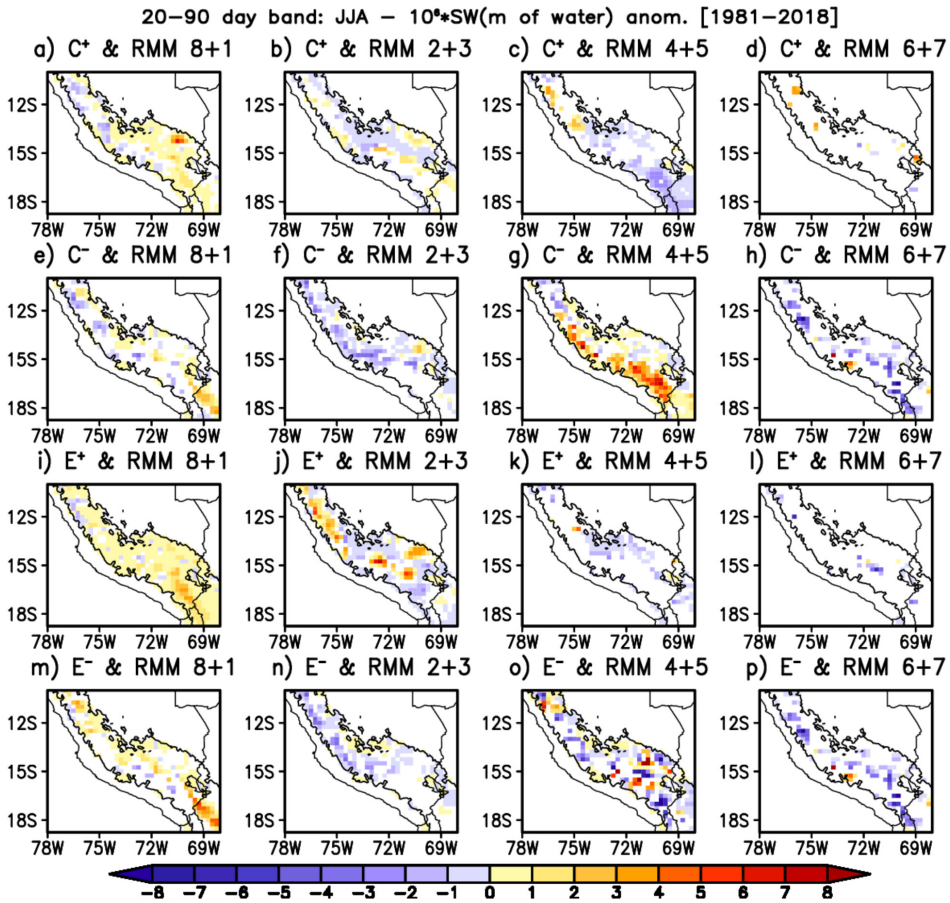

FIGURE 12 | Composite of filtered anomalies in the 20–90-day band for snowfall (m of water) over the Peruvian Andes for (a) RMM Phases 8+1, (b) RMM Phases 2+3, (c) RMM Phases 4+5, and (d) RMM Phases 6+7 under Central El Niño during austral winter (June–July–August, JJA). (e–h) As in (a–d) but for Central La Niña. (i–l) As in (a–d) but for Eastern El Niño. (m–p) As in (a–d) but for the Eastern La Niña. The shaded areas indicate significant snowfall anomalies at the 90% confidence level. The black contour represents the topographic elevation above 2500 m. The filtered snowfall anomalies were rescaled by a factor of 10^{-6}. The analysis is based on the period from 1981 to 2018. [Colour figure can be viewed at wileyonlinelibrary.com]

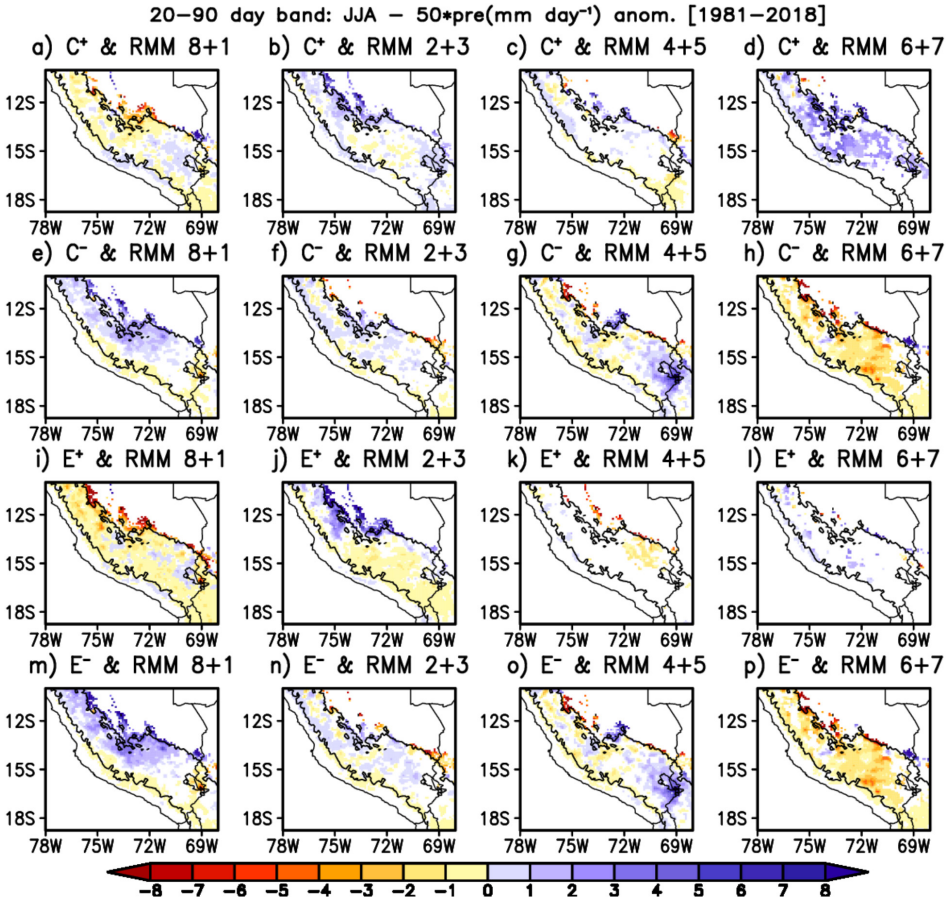

FIGURE 13 | Composite of filtered anomalies in the 20–90-day band for precipitation (mm day^{-1}) over the Peruvian Andes for (a) RMM Phases 8+1, (b) RMM Phases 2+3 (c) RMM Phases 4+5, and (d) RMM Phases 6+7 under the Central El Niño during austral winter (June–July–August, JJA). (e–h) As in (a–d) but for Central La Niña. (i–l) As in (a–d) but for Eastern El Niño. (m–p) As in (a–d) but for the Eastern La Niña. The shaded areas indicate significant precipitation anomalies at the 90% confidence level. The precipitation anomalies were rescaled by a factor of 50. The black contour represents the topographic elevation above 2500 m. The analysis is based on the period of 1981–2018. [Colour figure can be viewed at wileyonlinelibrary.com]

6.2 | Central La Niña

During Central La Niña, MJO Phases 2+3, and 6+7 reduce snowfall over the Peruvian Andes (Figure 12f,h). These reductions in snowfall agree with significant dry anomalies (Figure 13f,h) and significant positive OLR anomalies over the Peruvian Andes (Figure 14f,h). In contrast, during MJO Phases 8+1 and 4+5, snowfall increases in localised areas of the Peruvian Andes, but these phases exhibit different snowfall, precipitation, OLR and circulation patterns. For example, MJO Phases 8+1 result in increase in snowfall along the Eastern Cordillera of the central Peruvian Andes (Figure 12e). These increases in snowfall correspond to significant wet anomalies and negative OLR anomalies over the Eastern Cordillera of the central Peruvian Andes (Figures 13e and 14e). Non-significant easterly wind anomalies over the Peru result from an upper-level anticyclonic circulation anomaly over the southeastern Brazil (60° W, 24° S) at 200 hPa (Figure 15e). These upper-level easterly wind anomalies enhance moisture flow from the east, triggering convection over the southern Peruvian Andes, which leads to snowfall. However, no extreme snowfall events occur in the central Peruvian Andes during MJO Phases 8+1 under Central La Niña (Table 1). This suggests that the primary limiting factor is the lack of a strongly organised convection system over the Peruvian Andes. MJO Phases 4+5 induce snowfall along the Western Cordillera of the southern Peruvian Andes (Figure 12g). These increases in snowfall are associated with non-significant negative OLR anomalies over the Eastern Cordillera of the central Peruvian Andes (Figure 13g). However, the increase in snowfall is not consistent with the significant dry anomalies and upper-level westerly wind anomalies over the Western Cordillera of the southern Peruvian Andes at 200 hPa (Figures 14g and 15g). These significant westerly wind anomalies over the Peru result from an upper-level cyclonic circulation anomaly off the coast of Peru (82° W, 30° S) at 200 hPa (Figure 15g). These findings show that ERA5 reanalysis does not accurately capture the sign of the anomalies of the snowfall over the Peruvian Andes. Notably, no extreme snowfall events occur in the Peruvian Andes during MJO Phases 4+5 under Central La Niña (Table 1).

6.3 | Eastern El Niño

With respect to Eastern El Niño, MJO Phases 4+5 and 6+7 are associated with a reduction in snowfall in the Peruvian Andes (Figure 12k,l). Conversely, MJO Phases 8+1 and 2+3

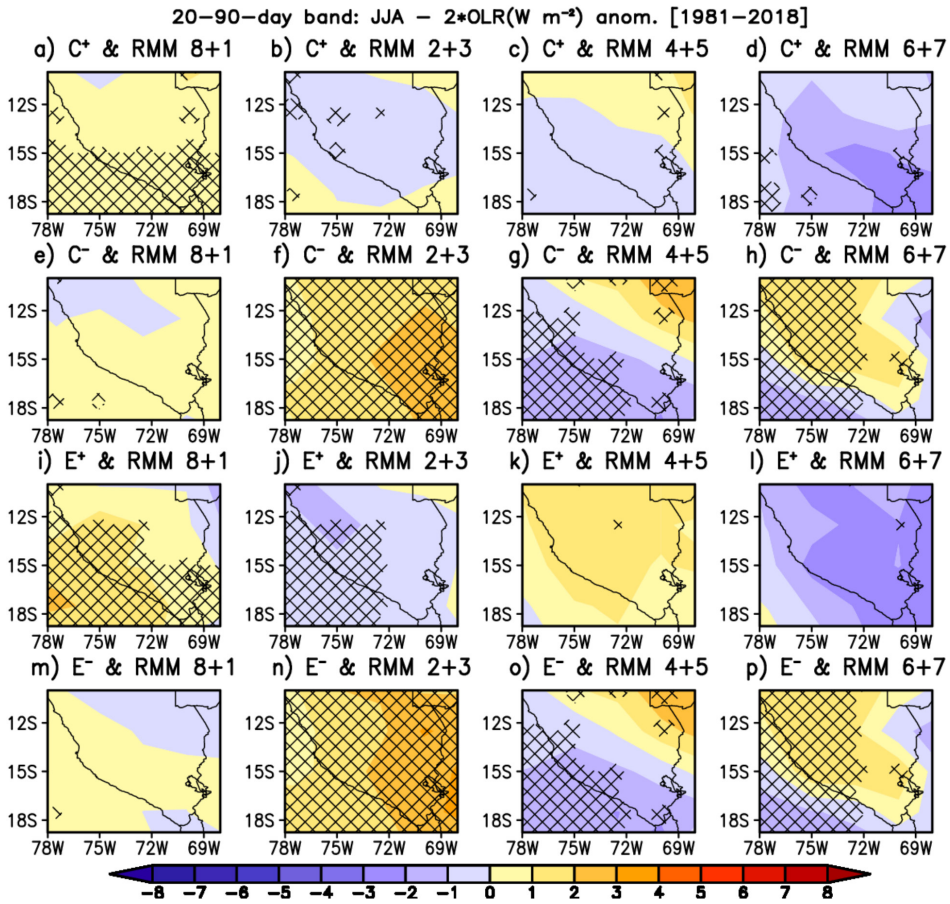

FIGURE 14 | Composite of filtered anomalies in the 20–90-day band for outgoing longwave radiation (OLR, W m^{-2}) over the Peruvian Andes for (a) RMM Phases 8 + 1, (b) RMM Phases 2 + 3, (c) RMM Phases 4 + 5, and (d) RMM Phases 6 + 7 under Central El Niño during austral winter (June–July–August, JJA). (e–h) As in (a–d) but for Central La Niña. (i–l) As in (a–d) but for Eastern El Niño. (m–p) As in (a–d) but for the Eastern La Niña. The shaded areas indicate significant OLR anomalies at the 90% confidence level. The black contour represents the topographic elevation above 2500 m. The analysis is based on the period from 1981 to 2018. [Colour figure can be viewed at wileyonlinelibrary.com]

cause positive snowfall anomalies over most of the Peruvian Andes (Figure 12i,j). However, they exhibit distinct snowfall, precipitation, OLR and circulation patterns. During MJO Phases 8 + 1, the increase in snowfall contradicts the observed significant dry anomalies and positive OLR anomalies over the Peruvian Andes, which extends toward the Bolivian Altiplano (Figures 13i and 14i). Significant westerly wind anomalies over the Peruvian Andes at 200 hPa weaken moisture flux from the east, which inhibits snowfall events. These finding show that the ERA5 reanalysis does not accurately reproduce the reduction in snowfall over the Peruvian Andes. Indeed, no extreme snowfall events occur in the Peruvian Andes during MJO Phases 8 + 1 under Eastern El Niño (Table 1). During MJO Phases 2 + 3, the increase in snowfall is consistent with the observed significant wet anomalies and negative OLR anomalies over the Eastern Cordillera of the central Peruvian Andes (Figures 13j and 14j). Significant easterly wind anomalies over the Peruvian Andes at 200 hPa indicate a strengthened moisture flux from the east, which triggers snowfall events. These upper-level easterly wind anomalies over Peru are part of an anticyclonic circulation over the central part of South Atlantic Ocean (40° W, 25° S) at 200 hPa. Based on these findings, the extreme snowfall event on August 08, 2008 (event 11, Table 1) was likely driven by enhanced moisture flux from the east and a strong convective organisation over the Peruvian Andes during MJO Phases 2 + 3, influenced by Eastern El Niño.

6.4 | Eastern La Niña

Under Eastern La Niña conditions, MJO Phases 2 + 3, 4 + 5, and 6 + 7 are associated with reduced snowfall over the Western Cordillera of the southern Peruvian Andes (Figure 12n–p). In contrast, MJO Phases 8 + 1 are associated with increased snowfall over the Eastern Cordillera of the central Peruvian Andes (Figure 12m). The positive snowfall anomalies are in agreement with the significant wet anomalies and negative OLR anomalies over the Eastern Cordillera of the central Peruvian Andes (Figures 13m and 14m). Easterly wind anomalies are observed over the Peru at 200 hPa but they are not statistically significant (Figure 15m). These easterly wind anomalies are part of an anticyclonic circulation over the central coast of Brazil (40° W, 23° S) at 200 hPa, suggesting that increased snowfall over the Eastern Cordillera in the central Peruvian Andes results from enhanced moisture flux from the Amazon Basin. Figure 15j also shows that the upper-level easterly wind anomalies over Peru are weaker than in the interaction between Eastern El Niño and RMM Phases 2 + 3. Based on these findings, the extreme

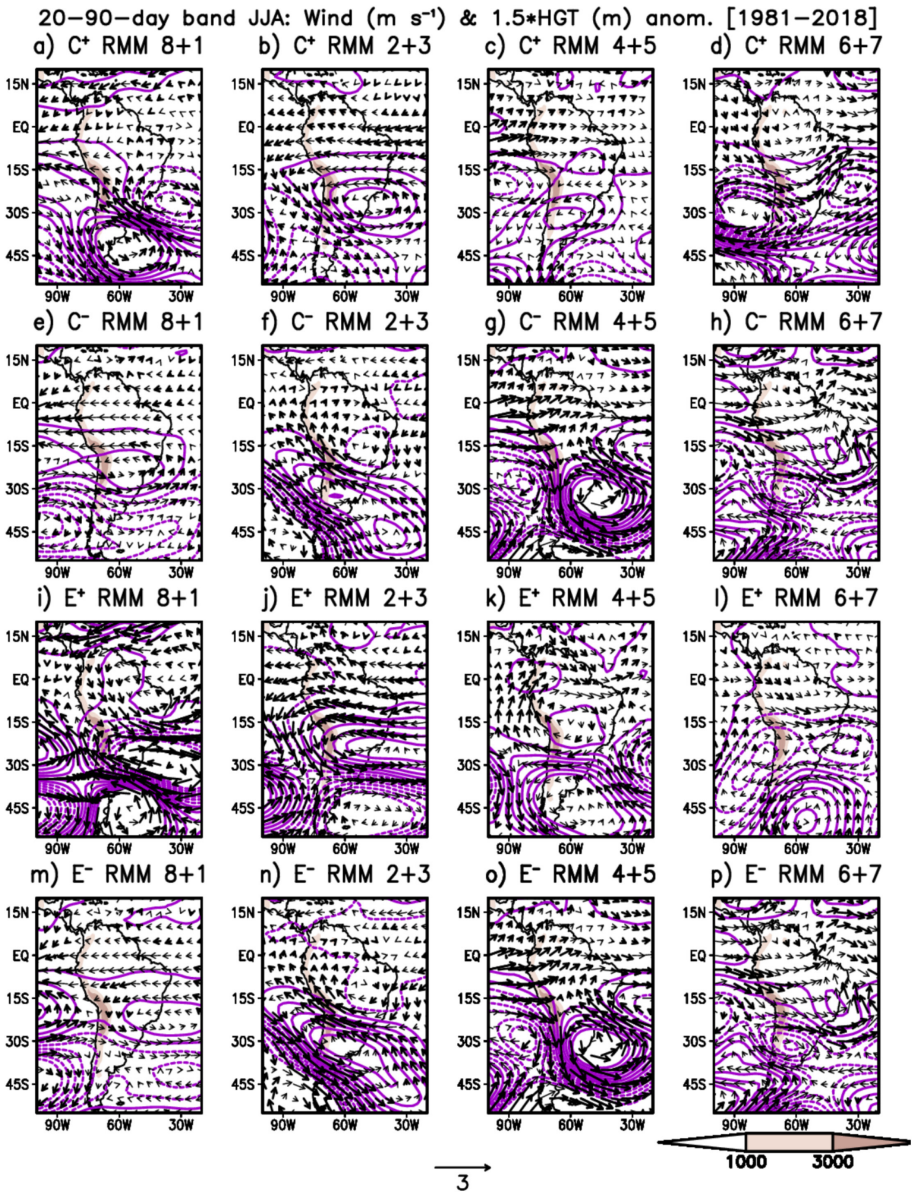

FIGURE 15 | Composite of filtered anomalies in the 20–90-day band for wind ($m\,s^{-1}$) and geopotential height (in m) anomalies over South America at 200 hPa for RMM Phases 8 + 1 under (a) Central El Niño, (e) Central La Niña, (i) Eastern El Niño and (m) Eastern La Niña during austral winter (June–July–August, JJA). (b, f, j and f) As in (a, e, i and m) but for RMM Phases 2 + 3. (c, g, k and o) As in (a, e, i and m) but for RMM Phases 4 + 5. (d, h, l and p) As in (a, e, i and m) but for RMM Phases 6 + 7. Only wind anomalies statistically significant at the 95% confidence level are shown. The shaded areas indicate significant OLR ($W\,m^{-2}$) anomalies at the 95% confidence level. The grey shading represents the topographic elevation above 1000 m. The geopotential height anomalies were rescaled by a factor of 2. The ERA5 reanalysis data from the period from 1981 to 2018 were used in this analysis. [Colour figure can be viewed at wileyonlinelibrary.com]

snowfall events on events 16–20 (Table 1) were likely caused by enhanced moisture flux from the east and a strong organisation of convection over the Eastern Cordillera of the central Peruvian Andes during MJO Phases 8 + 1, influenced by Eastern La Niña.

7 | Summary and Conclusions

This analysis documented the modulation effect of ENSO diversity on the impact of the MJO on extreme snowfall events in the Peruvian Andes during the austral summer (December, January, and February, DJF) and winter (June, July, and August, JJA) seasons from 1981 to 2018 using 31 × 31 km resolution ERA5 reanalysis data. The intraseasonal nature of extreme snowfall events in the Peruvian Andes is revealed by applying a bandpass filter of 20–90 day band. RMM and ENSO diversity indices were employed to elucidate the anomalous patterns of snowfall, precipitation, vertically integrated humidity transport, OLR, velocity potential, wind, and geopotential height over the Southern Hemisphere at 200 hPa associated with extreme snowfall events in the Peruvian Andes under different combinations of MJO and ENSO conditions for the identification of large-scale mechanisms.

An initial analysis revealed that the MJO modulates snowfall in the Peruvian Andes under non-ENSO conditions, but its

atmospheric circulation patterns change seasonally. During the DJF season, MJO Phases 2 + 3 induce snowfall in the Peruvian Andes through increased moisture flow from the east. This is achieved by reinforcing the upper-level BH-NL system, which is influenced by deep convection over the African continent and the Indian Ocean (Gahtan and Roundy 2021). Thus, the moisture mechanism is also effective during austral summer, leading to snowfall events in the Peruvian Andes. Conversely, during Phases 6 + 7, the MJO inhibits snowfall in the Peruvian Andes by causing upper-level southwesterly wind anomalies over Peru, thereby decreasing moisture flux from the east. These upper-level southwesterly wind anomalies over Peru are caused by the coupling of equatorial Kelvin and Rossby waves in the upper troposphere (Rui and Wang 1990; Roundy 2014; Sakaeda and Roundy 2015; Recalde-Coronel et al. 2020). However, the MJO cannot cause extreme snowfall events in the Peruvian Andes alone during the DJF season (see Table 1).

During the JJA season, MJO Phases 4 + 5 induce extreme snowfall events in the Western Cordillera of the southern Peruvian Andes caused by strengthened moisture flux from the east, driven by the equatorward propagation of an extratropical Rossby wave train along the coast of Brazil on intraseasonal timescales. MJO Phases 6 + 7 induce extreme snowfall events by intruding extratropical Rossby wave trains along the western side of the South American continent, reaching the central Andes at the upper troposphere level. This induces enough instability to fall snow in the Peruvian Andes. This is consistent with the mechanism for the winter snowfall events in the southern Peruvian Andes (Quispe and Avalos 2006a; Quispe and Avalos 2006b) and northern Chilean Andes (Vuille and Amman 1997).

With respect to ENSO diversity, during DJF season, the combined effect of the Central El Niño and MJO Phases 2 + 3 and 4 + 5 induces snowfall over the Western Cordillera of the southern Peruvian Andes by strengthening moisture flux from the east. This is driven by an enhanced upper-level BH-NL system over South America, which is reinforced by upper-level easterly flow anomalies resulting from deep convection over the African continent and the Indian Ocean (Chen et al. 1999; Gahtan and Roundy 2021). Central La Niña is associated with snowfall in the Western Cordillera of the Peruvian Andes during the DJF season. This occurs when its effect combines with MJO Phases 6 + 7, enhancing moisture flux from the east. This enhancement is caused by a southward shift of the upper-level Bolivian High, driven by the equatorial propagation of an upper-level extratropical Rossby wave train crossing the Altiplano region. The combined effect of Eastern El Niño and MJO Phases 4 + 5 and 6 + 7 induces snowfall over the Western Cordillera of the southern Peruvian Andes. This is facilitated by a strengthened moisture flux from the east, driven by an enhanced upper-level BH-NL system over South America as a response to the equatorward propagation of the extratropical Rossby wave train along the eastern coast of South America during the DJF season. The combined effect of Eastern La Niña and MJO Phases 4 + 5 results in increased snowfall over the southern Peruvian Andes during the DJF season. However, the absence of a well-organised convection system over the southern Peruvian Andes is the primary limiting factor for extreme snowfall events in this region, regardless of ENSO and the MJO during the DJF season.

During austral winter, the combined effect of the Central El Niño and MJO Phases 8 + 1 induces snowfall over the southern Peruvian Andes by enhancing moisture flux from the east. This is driven by enhanced upper-level easterly flow anomalies over the southern Peruvian Andes. These easterly wind anomalies are part of the equatorward propagation of an extratropical Rossby wave train along the eastern coast of Brazil at 200 hPa. Central La Niña is associated with snowfall in the Western Cordillera of the Peruvian Andes during the JJA season. This occurs when it interacts with MJO Phases 8 + 1, enhancing moisture flux from the east. However, these conditions do not lead to extreme snowfall events over the Peruvian Andes. The combined effect of Eastern El Niño and MJO Phases 2 + 3 induces snowfall over the Eastern Cordillera of the central Peruvian Andes by enhancing moisture flux from the east. This is driven by an enhanced upper-level easterly flow anomalies over the southern Peruvian Andes. These easterly wind anomalies over Peru are part of an anticyclonic circulation over the central part of South Atlantic Ocean (40° W, 25° S) at 200 hPa. The combined effect of Eastern La Niña and MJO Phases 8 + 1 increases snowfall over the Eastern Cordillera of the central Peruvian Andes during the JJA season by enhancing moisture flux from the east. This is driven by an enhanced upper-level easterly flow anomalies over Peru. These easterly wind anomalies are part of an anticyclonic circulation over the central coast of Brazil (40° W, 23° S) at 200 hPa. However, the lack of a strongly organised convection system over the Peruvian Andes is the main limiting factor for extreme snowfall events in this region, regardless of the possible combinations of ENSO and the MJO during the JJA season.

This study presented several limitations, such as the lack of long records of in situ snowfall data and the low performance of the ERA5 reanalysis. For example, the coarse horizontal resolution of the ERA5 reanalysis is only capable of simulating the intraseasonal winter pattern of extreme snowfall events across the Peruvian Andes. This is because the ERA5 reanalysis cannot accurately reproduce several local processes required to trigger extreme snowfall events in the Peruvian Andes. This finding suggests that further investigation into local phenomena is essential to better characterise extreme snowfall events in the Peruvian Andes during the austral summer and winter and mitigate their impacts on the local population.

Finally, these new outcomes will serve to improve the current prediction and monitoring systems for extreme snowfall events in the Peruvian Andes and thus reduce damage to the local population and their economic activities in the DJF and JJA seasons.

Author Contributions

Juan Sulca: conceptualization, methodology, formal analysis, investigation, funding acquisition, visualization, writing – original draft,

software, validation, project administration, writing – review and editing.

Acknowledgements

The author thanks Dr. Mayta for his comments on the initial version of the manuscript. This study was performed using computational resources, including the HPC Linux cluster, from the Laboratorio de Dinámica de Fluidos Geofísicos Computacionales at the Instituto Geofísico del Perú (grant 101-2014-FONDECYT). This work was subsidized by CONCYTEC through the PROCIENCIA Program under the framework of the contest "Scholarships in educational doctorate programs through inter-institutional partnerships", according to contract No. PE501093367-2024-PROCIENCIA-BM and the Interinstitutional Alliances Contest for Doctoral Programs, according to contract PE501084296-2023-PROCIENCIA-BM, as well as the Peruvian program PPR 068: Reducción de vulnerabilidad y atención de emergencias por desastres. [Correction added on 02 April 2025, after first online publication: The Acknowledgements section was updated in this version.]

Conflicts of Interest

The author declares no conflicts of interest.

Data Availability Statement

The data that support the findings of this study are openly available in PISCOpv2.1 at https://iridl.ldeo.columbia.edu/SOURCES/.SENAMHI/.HSR/.PISCO/.Prec/.v2p1/.unstable/.monthly/.Prec/.

References

Aliaga-Nestares, V., N. Goicochea-Díaz, T. Ita-Vargas, and N. Quispe-Gutiérrez. 2021. "Actualización del estudio de frecuencia de nevadas en el Perú." *Servicio Nacional de Meteorología e Hidrología*: 66. https://repositorio.senamhi.gob.pe/handle/20.500.12542/760.

Alvarez, M. S., C. S. Vera, G. N. Kiladis, and B. Liebmann. 2016. "Influence of the Madden–Julian Oscillation on South America's Precipitation and Surface Air Temperature." *Climate Dynamics* 46, no. 1: 245–262. https://doi.org/10.1007/s00382-015-2581-6.

Aybar, C., C. Fernandez, A. Huerta, W. Lavado, F. Vega, and O. Felipe-Obando. 2020. "Construction of a High-Resolution Gridded Rainfall Dataset for Peru From 1981 to the Present Day." *Hydrological Sciences Journal* 65: 770–785. https://doi.org/10.1080/02626667.2019.1649411.

Barreiro, M. 2016. "La Niña y sus teleconexiones." *Boletín técnico: Generación de información y Monitoreo del Fenómeno El Niño, Instituto Geofísico del Perú* 3, no. 8: 4–7.

Capotondi, A., A. T. Wittenberg, M. Newman, et al. 2015. "Understanding ENSO Diversity." *Bulletin of American Meteorology Society* 96: 921–938. https://doi.org/10.1175/BAMS-D-13-00117.1.

Chen, T. S., S. P. Weng, and S. Schubert. 1999. "Maintenance of Austral Summertime Upper-Tropospheric Circulation Over Tropical South America: The Bolivian High–Nordeste Low System." *Journal of Atmospheric Sciences* 56: 2081–2100. https://doi.org/10.1175/1520-0469(1999)056,2081:MOASUT.2.0.CO;2.

Fernandes, L. G., and A. M. Grimm. 2023. "ENSO Modulation of Global MJO and Its Impacts on South America." *Journal of Climate* 36, no. 22: 1–48. https://doi.org/10.1175/JCLI-D-22-0781.1.

Ferranti, L., T. N. Palmer, F. Molteni, and E. Klinker. 1990. "Tropical-Extratropical Interaction Associated With the 30-60 Day Oscillation and Its Impact on Medium and Extended Range Prediction." *Journal of Atmospheric Science* 47: 2177–2199. https://doi.org/10.1175/1520-0469(1990)047<2177:TEIAWT>2.0.CO;2.

Gahtan, J., and P. E. Roundy. 2021. "Meridional Movement of Geopotential Height Anomalies in the Subtropics and the Relationship to the Base-State Flow." *Quarterly Journal of the Royal Meteorological Society* 147: 627–646.

Garreaud, R. D. 1999. "Multiscale Analysis of the Summertime Precipitation Over the Central Andes." *Monthly Weather Review* 127: 901–921. https://doi.org/10.1175/1520-0493(1999)127,0901:MAOTSP.2.0.CO;2.

Garreaud, R., M. Vuille, and A. C. Clement. 2003. "The Climate of the Altiplano: Observed Current Conditions and Mechanisms of Past Changes." *Paleogeography, Paleoclimatology, Paleoecology* 194: 5–22. https://doi.org/10.1016/S0031-0182(03)00269-4.

Goudard, G., L. Limberger, and C. B. Carpenedo. 2024. "Influence of Eastern, Central and Mix El Niño on the Variability of Rainfall in Southeastern South America." *Frontiers in Earth Science* 12: 1134782. https://doi.org/10.3389/feart.2024.1134782.

Grimm, A. M. 2019. "Madden-Julian Oscillation on South American Summer Monsoon Season: Precipitation Anomalies, Extreme Events, Teleconnections, and Role in the MJO Cycle." *Climate Dynamics* 53: 907–932. https://doi.org/10.1007/s00382-019-04622-6.

Gutierrez, L., A. Camacho, C. Luis, E. Huanca, S. Marisol, and W. Lavado-Casimiro. 2022. High-Resolution Gridded Rainfall Dataset for Peru - PISCOp v2.1 Update. figshare. Dataset https://doi.org/10.6084/m9.figshare.21127423.v2.

Hersbach, H., B. Bell, P. Berrisford, et al. 2020. "The ERA5 Global Reanalysis." *Quarterly Journal of the Royal Meteorological Society* 146: 1999–2049. https://doi.org/10.1002/qj.3803.

Hurley, J. V., M. Vuille, D. R. Hardy, S. Burns, and L. G. Thompson. 2015. "Cold Air Incursions, δ18O Variability and Monsoon Dynamics Associated With Snow Days at Quelccaya Ice Cap. Peru." *Journal of Geophysical Research* 120: 7467–7487. https://doi.org/10.1002/2015JD023323.

Imfeld, N., C. Barreto Schuler, K. M. Correa Marrou, et al. 2019. "Summertime Precipitation Deficits in the Southern Peruvian Highlands Since 1964." *International Journal of Climatology* 39: 4497–4513. https://doi.org/10.1002/joc.6087.

IRI. 2024. The Real-Time Multivariate MJO Index. (December 02, 2024). https://iridl.ldeo.columbia.edu/SOURCES/.BoM/.MJO/.RMM/index.html?Set-Language=en.

Kodama, Y. 1992. "Large-Scale Common Features of Subtropical Precipitation Zones (the Baiu Frontal Zone, the SPCZ and the SACZ). Part I: Characteristics of Subtropical Frontal Zones." *Journal of the Meteorological Society of Japan* 70, no. 4: 813–836. https://doi.org/10.2151/jmsj1965.70.4_813.

Labat, D., J. Ronchail, and J. L. Guyot. 2005. "Recent Advances in Wavelet Analyses: Part 2—Amazon, Parana, Orinoco and Congo Discharges Time Scale Variability." *Journal of Hydrology* 314, no. 1–4: 289–311. https://doi.org/10.1016/j.jhydrol.2005.04.004.

Labat, D., J. C. Espinoza, J. Ronchail, et al. 2012. "Fluctuations in the Monthly Discharge of Guyana Shield Rivers, Related to Pacific and Atlantic Climate Variability." *Hydrological Sciences Journal* 57, no. 6: 1–11. https://doi.org/10.1080/02626667.2012.695074.

Lagos, P., Y. Silva, E. Nickl, and K. Mosquera. 2008. "El Niño Related Precipitation Variability in Peru." *Advances in Geosciences* 14: 231–237. https://doi.org/10.5194/adgeo-14-231-2008.

Lenters, J. D., and K. H. Cook. 1997. "On the Origin of the Bolivian High and Related Circulation Features of the South American Climate." *Journal of the Atmospheric Sciences* 54: 656–677. https://doi.org/10.1175/1520-0469(1997)054⟨0656:OTOOTB⟩2.0.CO;2.

Liebmann, B., and C. A. Smith. 1996. "Description of a Complete (Interpolated) Outgoing Longwave Radiation Dataset." *Bulletin of the American Meteorological Society* 77: 1275–1277.

Liebmann, B., G. N. Kiladis, J. A. Marengo, T. Ambrizzi, and J. Glick. 1999. "Submonthly Convective Variability Over South America

and the South Atlantic Convergence Zone." *Journal of Climate* 12: 1877–1891. https://doi.org/10.1175/1520-0442(1999)012⟨1877:SCVOSA⟩2.0.CO;2.

Liu, N., C. Liu, and T. Lavigne. 2019. "The Variation of the Intensity, Height, and Size of Precipitation Systems With El Niño-Southern Oscillation in the Tropics and Subtropics." *Journal of Climate* 32: 4281–4297. https://doi.org/10.1175/JCLI-D-18-0766.1.

Liu, F., B. Wang, Y. Ouyang, et al. 2023. "Intraseasonal Variability of Global Land Monsoon Precipitation and Its Recent Trend." *NPJ Climate and Atmospheric Science* 5, no. 30: 1–12. https://doi.org/10.1038/s41612-022-00253-7.

Madden, R. A., and P. R. Julian. 1972. "Description of Global-Scale Circulation Cells in the Tropics With a 40–50-Day Period." *Journal of Atmospheric Sciences* 29: 1109–1123. https://doi.org/10.1175/1520-0469(1972)029<1109:DOGSCC>2.0.CO;2.

Madden, R. A., and P. R. Julian. 1994. "Observations of the 40–50-Day Tropical Oscillation: A Review." *Monthly Weather Review* 122: 814–837. https://doi.org/10.1175/1520-0493(1994)122<0814:OOTDTO>2.0.CO;2.

Mayta, V. C., T. Ambrizzi, J. C. Espinoza, and P. L. Silva Días. 2019. "The Role of the Madden–Julian Oscillation on the Amazon Basin Intraseasonal Rainfall Variability." *International Journal of Climatology* 39: 343–360. https://doi.org/10.1002/joc.5810.

Montini, T. L., C. Jones, and L. M. Carvalho. 2019. "The South American Low-Level Jet: A New Climatology, Variability, and Changes." *Journal of Geophysical Research: Atmospheres* 124: 1200–1218. https://doi.org/10.1029/2018JD029634.

Moon, J.-Y., B. Wang, and K.-J. Ha. 2011. "ENSO Regulation of MJO Teleconnection." *Climate Dynamics* 37: 1133–1149. https://doi.org/10.1007/s00382-010-0902-3.

Quispe, N. 2014. "Evaluación Climático de la Depresión Aislada en Niveles Altos (DANA) Sobre Sudamérica y Océanos Adyacentes y Estudio de un Caso en el Pacifico Oriental." In *M.S. Thesis*, Universidad Nacional Agraria La Molina, 151 p.

Quispe, K. 2017. "Patrones Sinópticos de Una Dana Asociados a la Ocurrencia de Nevadas en la Sierra Central y Sur del Perú (in Spanish)." Ingeniero Meteorólogo, Facultad de Ciencias, Universidad Nacional Agraria La Molina, 82 pp. http://repositorio.lamolina.edu.pe/handle/UNALM/3632.

Quispe, N., and G. Avalos. 2006a. "Intense Snowstorm in the Southern Mountains of Peru Associated to the Incursion of Cut-Off Low-Pressure Systems at Upper-Level." In *ICSHMO Proceedings of 8 ICSHMO, Foz do Iguaçu, Brazil*, April 24–28, 2006, INPE, 1945–1958.

Quispe, N., and G. Avalos. 2006b. "Intense Snowstorm in the Southern Mountains of Peru Associated to the Incursion of Cut-Off Low-Pressure Systems at Upper Level." In *Proc. 8th Int. Conf. on Southern Hemisphere Meteorology and Oceanography (ICSHMO)*, INPE, 1945–1948.

Recalde-Coronel, G. C., B. Zaitchik, and W. K. Pan. 2020. "Madden–Julian Oscillation Influence on Subseasonal Rainfall Variability on the West of South America." *Climate Dynamics* 54, no. 3–4: 2167–2185. https://doi.org/10.1007/s00382-019-05107-2.

Roundy, P. 2014. "Some Aspects of Western Hemisphere Circulation and the Madden-Julian Oscillation." *Journal of the Atmospheric Sciences* 71: 2027–2039. https://doi.org/10.1175/JAS-D-13-0210.1.

Rui, H., and B. Wang. 1990. "Development Characteristics and Dynamic Structure of Tropical Intraseasonal Convection Anomalies." *Journal of Atmospheric Science* 47, no. 3: 357–379. https://doi.org/10.1175/1520-0469(1990)047<0357:DCADSO>2.0.CO;2.

Sakaeda, N., and P. E. Roundy. 2015. "The Development of Upper-Tropospheric Wind Over the Western Hemisphere in Association With MJO Convective Initiation." *Journal of Atmospheric Science* 72: 3138–3160. https://doi.org/10.1175/JAS-D-14-0293.1.

Satoh, S., K. Furukawa, Y. Senbokuya, et al. 2004. "Development of Spaceborne Dual-Frequency Precipitation Radar for the Global Precipitation Measurement." IGARSS 2004. September 2004. IEEE International Geoscience and Remote Sensing Symposium. https://doi.org/10.1109/IGARSS.2004.1370481.

Segura, H., C. Junquas, J. C. Espinoza, et al. 2019. "New Insights Into the Rainfall Variability in the Tropical Andes on Seasonal and Interannual Time Scales." *Climate Dynamics* 53: 405–426. https://doi.org/10.1007/s00382-018-4590-8.

Segura, H., J. C. Espinoza, C. Junquas, T. Lebel, M. Vuille, and T. Condom. 2022. "Extreme Austral Winter Precipitation Events Over the South-American Altiplano: Regional Atmospheric Features." *Climate Dynamics* 59, no. 9-10: 3069–3086. https://doi.org/10.1007/s00382-022-06240-1.

Shimizu, M. H., and T. Ambrizzi. 2016. "MJO Influence on ENSO Effects in Precipitation and Temperature Over South America." *Theorical and Applied Climatology* 124: 291–301. https://doi.org/10.1007/s00704-015-1421-2.

Shimizu, M. H., T. Ambrizzi, and B. Liebmann. 2017. "Extreme Precipitation Events and Their Relationship With ENSO and MJO Phases Over Northern South America." *International Journal of Climatology* 37: 2977–2989. https://doi.org/10.1002/joc.4893.

Sulca, J., M. Vuille, Y. Silva, and K. Takahashi. 2016. "Teleconnections Between the Peruvian Central Andes and Northeast Brazil During Extreme Rainfall Events." *Journal of Hydrometeorology* 17: 499–515. https://doi.org/10.1175/JHM-D-15-0034.1.

Sulca, J., M. Vuille, O. Ellison-Timm, B. Dong, and R. Zubieta. 2021. "Empirical-statistical Downscaling of Austral Summer Precipitation Over South America, With a Focus on the Central Peruvian Andes and the Equatorial Amazon Basin." *Journal of Applied Meteorology and Climatology* 60: 65–85. https://doi.org/10.1175/JAMC-D-20-0066.1.

Sulca, J., K. Takahashi, J. C. Espinoza, M. Vuille, and W. Lavado-Casimiro. 2018. "Impacts of Different ENSO Flavors and Tropical Pacific Convection Variability (ITCZ, SPCZ) on Austral Summer Rainfall in South America, With a Focus on Peru." *International Journal of Climatology* 38, no. 1: 420–435. https://doi.org/10.1002/joc.5185.

Sulca, J., K. Takahashi, J. Tacza, J. C. Espinoza, and B. Dong. 2022. "Decadal Variability in the Austral Summer Precipitation Over the Central Andes: Observations and the Empirical-Statistical Downscaling Model." *International Journal of Climatology* 42, no. 16: 9836–9864. https://doi.org/10.1002/joc.7867.

Sulca, J., K. Takahashi, and J. Tacza. 2024b. "Variabilidad bienal e interanual de la temperatura superficial del mar de la región tropical de los océanos Pacífico y Atlántico." *Boletín científico El Niño, Instituto Geofísico del Perú* 11, no. 1: 12–17.

Sulca, J., K. Takahashi, J. C. Espinoza, et al. 2024a. "A Multiple Linear Regression Model for the Prediction of Summer Rainfall in the Northwestern Peruvian Amazon Using Large-Scale Indices." *Climate Dynamics* 62: 4431–4451. https://doi.org/10.1007/s00382-023-07044-7.

Takahashi, K., A. Montecinos, K. Goubanova, and B. Dewitte. 2011. "ENSO Regimes: Reinterpreting the Canonical and Modoki El Niño." *Geophysical Research Letters* 38: L10704. https://doi.org/10.1029/2011GL047364.

Tedeschi, R. G., A. M. Grimm, and I. F. A. Cavalcanti. 2015. "Influence of Central and East ENSO on Extreme Events of Precipitation in South America During Austral Spring and Summer." *International Journal of Climatology* 35: 2045–2064. https://doi.org/10.1002/joc.4106.

Tedeschi, R. G., A. M. Grimm, and I. F. A. Cavalcanti. 2016. "Influence of Central and East ENSO on Precipitation and its Extreme Events in South America during Austral Autumn and Winter." *International Journal of Climatology* 36: 4797–4814. https://doi.org/10.1002/joc.4670.

Torrence, C., and G. P. Compo. 1998. "A Practical Guide to Wavelet Analysis." *Bulletin of the American Meteorology Society* 79, no. 1:

61–78. https://doi.org/10.1175/1520-0477(1998)079<0061:APGTWA>2.0.CO;2.

Villalobos-Puma, E., J. L. Flores-Rojas, D. Martinez-Castro, et al. 2022. "Summertime Precipitation Extremes and the Influence of Atmospheric Flows on the Western Slopes of the Southern Andes of Perú." *International Journal of Climatology* 42, no. 16: 9909–9930. https://doi.org/10.1002/joc.7871.

Vuille, M., and C. Ammann. 1997. "Regional Snowfall Pattern in the High, and Andes (South America)." *Climatic Change* 36: 413–423.

Vuille, M., R. S. Bradley, and F. Keimig. 2000. "Interannual Climate Variability in the Central Andes and Its Relation to Tropical Pacific and Atlantic Forcing." *Journal of Geophysical Research* 105: 12447–12460. https://doi.org/10.1029/2000JD900134.

Vuille, M., and F. Keimig. 2004. "Interannual Variability of Summertime Convective Cloudiness and Precipitation in the Central Andes Derived from ISCCP-B3 Data." *Journal of Climate* 17: 3334–3348. https://doi.org/10.1175/1520-0442(2004)017⟨3334:IVOSCC⟩2.0.CO;2.

Vuille, M., B. Francou, P. Wagnon, et al. 2008. "Climate Change and Tropical Andean Glaciers – Past, Present and Future." *Earth-Science Reviews* 89: 79–96. https://doi.org/10.1016/j.earscirev.2008.04.002.

Webster, P. J., and J. R. Holton. 1982. "Cross-Equatorial Response to Middle-Latitude Forcing in a Zonally Varying Basic State." *Journal of Atmospheric Science* 39: 722–733. https://doi.org/10.1175/1520-0469(1982)039<0722:CERTML>2.0.CO;2.

Wheeler, M. C., and H. H. Hendon. 2004. "An All-Season Real-Time Multivariate MJO Index: Development of an Index for Monitoring and Prediction." *Monthly Weather Review* 132: 1917–1932. https://doi.org/10.1175/1520-0493(2004)132<1917:AARMMI>2.0.CO;2.

Wilks, S. D. 2011. "Statistical Methods in the Atmospheric Sciences." In *International Geophysics Series*, edited by R. Dmowska, D. Hartmann, and H. T. Rossby, vol. 100. Academic Press.

Wu, S., M. Notaro, S. Vavrus, et al. 2018. "Efficacy of Tendency and Linear Inverse Models to Predict Southern Peru's Rainy Season Precipitation." *International Journal of Climatology* 38: 2590–2604. https://doi.org/10.1002/joc.5442.